Titanium Niobium Oxide: From Discovery to Application in Fast-Charging Lithium-ion Batteries

Kent J. Griffith,[1*] Yasuhiro Harada,[2] Shun Egusa,[3] Rogério M. Ribas,[4] Robson S. Monteiro,[4] Robert B. Von Dreele,[5] Anthony K. Cheetham,[6] R. J. Cava,[7] Clare P. Grey,[8] John B. Goodenough[9]

[1]Department of Chemistry and Department of Materials Science and Engineering, Northwestern University, Evanston, Illinois 60208, United States
[2]Corporate Research & Development Center, Toshiba Corporation, Kawasaki 212-8582, Japan
[3]Battery Business Division, Toshiba Corporation, Kawasaki 212-8585, Japan
[4]Companhia Brasileira de Metalurgia e Mineração (CBMM), Araxá, Minas Gerais 38183-903, Brazil
[5]Argonne National Laboratory, Argonne, Illinois 60439, United States
[6]Materials Research Laboratory, University of California, Santa Barbara, California 93106, United States
[7]Department of Chemistry, Princeton University, Princeton, New Jersey 08544, United States
[8]Department of Chemistry, University of Cambridge, Cambridge CB2 1EW, United Kingdom
[9]Materials Science and Engineering Program and Texas Materials Institute, University of Texas at Austin, Austin, Texas 78712, United States
[*]Corresponding Author

Abstract
Lithium-ion batteries are essential for portable technology and are now poised to disrupt a century of combustion-based transportation. The electrification revolution could eliminate our reliance on fossil fuels and enable a clean energy future; advanced batteries would facilitate this transition. However, owing to the demanding performance, cost, and safety requirements, it is challenging to translate new materials from laboratory prototypes to industrial-scale products. This Perspective describes that journey for a new lithium-ion battery anode material, $TiNb_2O_7$ (TNO). TNO is intended as an alternative to graphite or $Li_4Ti_5O_{12}$ with better rate and safety characteristics than the former, and higher energy density than the latter. The high capacity of TNO stems from multielectron redox of Nb^{5+} to Nb^{3+}, its operating voltage window well above Li^+/Li reduction potential prevents lithium dendrite formation, and its open crystal structure leads to high-power performance. Nevertheless, the creation of a practical TNO anode was non-linear and non-trivial. Its history is built on 30 years on fundamental science that preceded its application as a battery, and its battery development included a nearly 30-year gap. The insights and lessons contained in this Perspective, many of them acquired firsthand, serve two purposes: (i) to unite the disparate

studies of $TiNb_2O_7$ into a coherent modern understanding relevant to its application as a battery material and (ii) to briefly highlight some of the challenges faced when scaling up a new material that affect $TiNb_2O_7$, as well as new electrode candidates more generally.

1. Introduction. Of the thousands of materials that have been investigated as prospective rechargeable lithium-ion battery electrodes, only a handful have progressed along the road to commercialization. For cathodes, the list comprises layered rocksalt-derived lithium cobalt oxide (LCO, $LiCoO_2$),[1] olivine lithium iron phosphate (LFP, $LiFePO_4$),[2] spinel lithium manganese oxide (LMO, $LiMn_2O_4$),[3] and their many substituted variations, particularly for the layered rock-salt phases. For anodes, there have been even fewer successes, with graphite and spinel lithium titanium oxide (LTO, $Li_4Ti_5O_{12}$)[4] breaking through. Silicon-based anode materials (Si, SiO_x) are being developed for commercialization by many start-up companies, and silicon compounds are finding use as an additive to graphite, but they have not as yet found large-scale adoption as primarily silicon anodes when long cycle life is required. Lithium metal was initially considered as an anode for commercial lithium-shuttling batteries, but it was quickly pulled from the market due to safety issues arising from lithium dendrites, though it is still commercialized for elevated temperature use with a polymer electrolyte.[5] Descriptions of the development of these materials can be found elsewhere.[6–19] Titanium niobium oxide (TNO, $TiNb_2O_7$), with many characteristics that are similar to LTO, is an electrode material with a crystallographic shear structure (Figure 1) that can be used as a high-power anode. Following the award of the 2019 Nobel Prize in Chemistry to Whittingham, Goodenough, and Yoshino "for the development of lithium-ion batteries",[7] and owing to the global effort to develop advanced battery materials, we thought it would be timely to chronicle and illustrate some of the challenges associated with the scale-up and building of the commercial titanium niobium oxide TNO – based battery, combining contributions from authors involved in the early discoveries, more recent fundamental studies, and researchers involved in its commercial development (see COI statements).

This perspective commences with the discovery and characterization of $TiNb_2O_7$, follows the first mAh half-cell tests in research laboratories, details the tortuous path toward a practical large-scale battery cell, and concludes with a brief future outlook for this new battery and its related chemistries. The historical account of fundamental studies on $TiNb_2O_7$ sets the stage for understanding how its crystal structure, cation order, and defects affect its performance as a battery

electrode; though it is also noteworthy that these studies in $TiNb_2O_7$ were closely tied to the development of now ubiquitous techniques such as Rietveld refinement, neutron diffraction, and transmission electron microscopy. We hope that an understanding of the commercialization journey of $TiNb_2O_7$ and the interplay between fundamental and industrially driven studies may help speed up the transition of other new electrode materials into the marketplace for an increasingly diverse range of battery applications.
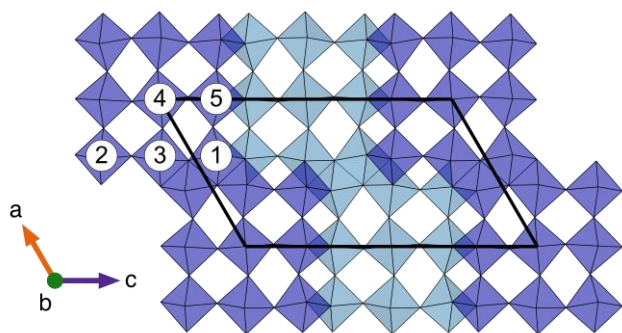
Figure 1. Crystal structure of $TiNb_2O_7$ showing $(Ti/Nb)O_6$ octahedra arranged into 3×3 blocks; light and dark blocks are offset by ½ octahedra in the *b*-axis. A monoclinic unit cell is outlined in black. The crystallographically distinct cation sites are labeled; an inversion center exists in the block center.

Electrochemical energy storage technologies come with trade-offs; there is no known holy grail. Thus, new lithium-ion battery materials typically target some subset of voltage, chemical compatibility, mechanical stability, safety, sustainability, material cost, manufacturing cost, capacity, and energy and power density requirements while maintaining acceptable trade-offs among others. Many of the same choices are made at the electrode, cell, and battery pack levels. This process leads to different solutions for different applications, broadly divided into either high power density or high energy density cells, where the requirement may either be volumetric or gravimetric. In addition to the above requirements, characteristics to consider for successful commercialization include fast charging capability, shelf life, and operational temperature window. These considerations, in particular its energy density, rapid lithium diffusion and a potential window of 1.0–2.0 V vs. Li^+/Li, make $TiNb_2O_7$ suitable as an anode material in the design of a safe battery that can offer high discharge power, rapid charging, and a long cycle life.

The state-of-the-art material in the high-power and fast-charging performance space is an LTO-related compound, commercialized by Toshiba as the SCiB™ battery[20], which is now used globally in applications including mild-hybrid electric passenger cars, electric buses and trolleys, electric trains, and grid energy storage systems. Generally speaking, $Li_4Ti_5O_{12}$ reacts with lithium in a two-phase intercalation reaction to form $Li_7Ti_5O_{12}$ with an average intercalation voltage of

1.55 V and a theoretical capacity of 175.1 mAh·g^{-1}. Relative to graphite, anodes of $Li_4Ti_5O_{12}$ provide only 50% of the gravimetric capacity and sacrifice approximately 40% of the voltage when paired with a 4.0 V cathode. Despite their limited energy density, LTO-based cells have had commercial success because they can be cycled over 20,000 times and can operate safely at current densities and temperatures that are not suitable for graphite-based batteries.[20] Still, $Li_4Ti_5O_{12}$ has only captured a small percentage of the anode market share, with a 2020 market size of approximately 12,000 tons.[21]

New materials with high power and higher energy density are required. Titanium(IV)-based materials have been extensively investigated for this purpose owing to their light masses and suitable voltage ranges. TiO_2, in particular, offers a theoretical capacity of 335.6 mAh·g^{-1} for the reaction to $LiTiO_2$ and a range of polymorphs including rutile, anatase, brookite, and bronze, but none of these have penetrated the commercial market. Niobium(V), at first glance, is less favorable due to its higher mass, but this disadvantage is more than fully compensated by an accessible two-electron reduction to Nb(III), a critical driver in this story and the broader recent acceleration of niobium-based battery research.

In the context of battery materials, niobium(V) possesses many of the attractive features of titanium(IV). It is redox active, non-toxic, and air- and water-stable when in an oxide. While neither niobium(V) nor titanium(IV) yield electronically conductive materials because they are d^0 ions, the expanded $4d$ orbitals of niobium provide better orbital overlap for electron delocalization upon the introduction of charge carriers (e.g. by extrinsic doping or *in situ* from lithiation) whereas carrier doping of titanium(IV) oxides typically results in lower mobility materials, possibly due to the tendency to form polarons.[22,23] From the perspective of availability, the average concentration of niobium in the upper continental crust is 10–26 ppm, comparable to cobalt (10–18 ppm), nickel (19–60 ppm), copper (14–32 ppm), molybdenum (0.6–1.5 ppm), tungsten (0.9–3.3 ppm), tin (1.7–5.5 ppm), lithium (20–41 ppm), vanadium (53–107 ppm), and zinc (52–75 ppm) but far less than Mn (600–735 ppm), Ti (0.45%), and Fe (4.1–4.7%).[24] In terms of the impact of the readiness of the niobium industry for battery materials, an estimated 74,000 tons of niobium was produced in 2019, but the reserves (*i.e.* economic resources, not total resources) were more than 13,000,000 tons.[25,26] According to the U.S. Geological Survey, "[w]orld resources of niobium are more than adequate to supply projected needs."[26] However, niobium is considered a critical element owing to its concentrated production, which is estimated at 88% from Brazil, primarily from one

company, and 10% from Canada, also primarily from one company.[25–28] The U.S. Geological Survey also reports that the Elk Creek deposit in Nebraska, United States, is expected to produce niobium after 2020.[26]

Owing to the favorable properties of niobium, $TiNb_2O_7$ is being developed as a high energy density alternative anode material to $Li_4Ti_5O_{12}$ for specific market sectors. The reaction of $TiNb_2O_7$ with lithium is not as well defined as that of $Li_4Ti_5O_{12}$ because it occurs over a sloping voltage profile without a steep voltage drop. The reduction to $Li_3Ti^{III}Nb^{IV}_2O_7$ (one lithium per transition metal) occurs at circa 1.4 V vs. Li^+/Li, providing a theoretical capacity of 232.6 $mAh·g^{-1}$. The reaction proceeds further as the voltage is decreased and can proceed all the way to $Li_5Ti^{III}Nb^{III}_2O_7$ with a theoretical capacity of 387.7 $mAh·g^{-1}$.[29–31] The multielectron redox chemistry of $TiNb_2O_7$ puts it on a par with the gravimetric capacity of graphite (371.9 $mAh·g^{-1}$). It is worth mentioning that the crystal densities of $Li_4Ti_5O_{12}$ (3.48 $g·cm^{-3}$)[32] and $TiNb_2O_7$ (4.33 $g·cm^{-3}$)[33] are 1.6 and 2.0 times that of graphite (2.22 $g·cm^{-3}$),[34] respectively; thus, the volumetric energy densities of these oxide anodes may compare to graphite more favorably than their gravimetric energy densities, depending on microstructural and electrode considerations. This point is particularly important because gravimetric performance is far easier to quantify with thin films and small cells than volumetric performance, but the latter is more critical for most applications. By way of example, decreasing the weight of a battery by 20% may reduce the weight of an EV by about 5% and thus improve its driving range by a few percent. On the other hand, decreasing the volume of the battery by 20% enables a 25% increase in the number of cells and energy resulting in a nearly 25% increase in driving range. If the capacity of $TiNb_2O_7$ reaches parity with graphite, then it offers a clear advantage over $Li_4Ti_5O_{12}$ and should approach graphite on a volumetric energy basis. The high voltage of anodes such as $TiNb_2O_7$ and $Li_4Ti_5O_{12}$ has both problematic and advantageous consequences. The cell-level energy density suffers significantly from the large loss in cell voltage, but the proclivity to form Li dendrites on fast charging is suppressed because the voltage is well above the lithium plating potential. Thus, a high anode voltage enables safe charging under high current densities even in a heterogeneous electrode with large overpotentials and may be considered a necessary feature for very rapid charging. The high operating voltage may also mitigate surface–electrolyte interphase (SEI) formation as the voltage window is largely within the stability limits of standard electrolytes.

2. Historical Background: 1950–2010. 2.1 Discovery and Structural Solution. A phase with the composition $TiNb_2O_7$ was first reported in late 1952 during a study of refractory oxides for nuclear engineering applications at the Battelle Memorial Institute in Columbus, Ohio.[35,36] Three years later, Robert Roth and L. W. Coughanour at the National Bureau of Standards (now the National Institute of Standards and Technology) in Gaithersburg Maryland, published the first TiO_2–Nb_2O_5 phase diagram.[37] In their original report, X-ray analyses suggested that "TiO_2:$3Nb_2O_5$ and TiO_2:Nb_2O_5 are probably pure compounds" and that rutile TiO_2 and H-Nb_2O_5 end-members both have solid-solution regions of more than mol 10%[37]. However, it was later revealed that the phase diagram is more complex: "TiO_2:$3Nb_2O_5$" was actually $Ti_2Nb_{10}O_{29}$,[38] a phase $TiNb_{24}O_{62}$ exists[39], and the solid-solution region of TiO_2 in H-Nb_2O_5 is in fact quite narrow.[40–42] In 1961, six years after the report from Roth and Coughanour, A. David Wadsley at the Commonwealth Scientific and Industrial Research Organisation (CSIRO) in Canberra presented the first full structural model of $TiNb_2O_7$.[43] The crystal structure of $TiNb_2O_7$ proved to be monumental, the first of what came to be known as block phases and eventually Wadsley–Roth phases, based on the principle of crystallographic shear[44,45] of ReO_3-like,[46] i.e. unfilled perovskite, blocks (see Section 3.2.1). Wadsley already began to describe $TiNb_2O_7$ as a shear structure by 1958[44], having previously used the term molecular shear to describe the $(Mo,W)_nO_{3n-1}$ homologous series.[47] Over the 1960s, until his untimely death, Wadsley, together with Roth, would go on to demonstrate that this structure type accounts for the "nonstoichiometry" (relative to a 3:1 O:M ratio required for the ReO_3 structure) across the TiO_2–Nb_2O_5 series,[38,39] for the high temperature phase of Nb_2O_5,[48] for PNb_9O_{25},[49] and for niobium-rich compositions within the Nb_2O_5–WO_3 phase diagram[50–56]. Blocks formed from ordered, orthogonal crystallographic shear planes in an ReO_3-like structure give rise to a series of substoichiometric MO_{3-x} line phases with "a specific, albeit obscure, stoichiometry"[57]. Wadsley, in his final work, remarked that "The formula thus derived [from crystal structure analysis] may appear cumbersome, but it is nevertheless preferable to a less descriptive one based on a fractional ratio of oxygen to metal."[58] The block concept was extended to show that even subtle changes in stoichiometry near the line compounds can be explained by the coherent intergrowth of block structures.[58–61] It was proposed that this is a low energy process because local structure and bonding are unaltered, unlike the case for the point defect models favored at the time to explain the M:O ratios in these phases. That these shear planes form long-range ordered arrays was a surprise because it means that they interact coherently over a length

scale of tens of Ångstroms. While the block principles are now widely accepted, this structural mechanism was heavily debated and did not begin to settle until the structural solution of $TiNb_2O_7$.

2.2 Defect Chemistry. The block mechanism with periodic and orthogonal shear planes describes the idealized structure of $TiNb_2O_7$. Real crystals, however, exhibit defects. Extended planar intergrowth defects, known as Wadsley defects,[62,63] have been described in TiO_2–Nb_2O_5 and Nb_2O_5–WO_3 block phases and are sensitive to factors such as composition, temperature, time, and atmosphere. John Allpress, a contemporary of Wadsley at CSIRO, undertook defect studies of $TiNb_2O_7$ among other shear phases in early electron microscopy studies in the late 1960s and early 1970s. It turned out that the key features—the alternating filled columns and empty tunnels—of the Nb_2O_5-related block structures were extremely well-matched to the resolution of the latest transmission electron microscopy (TEM) methods at that time, so there was a great deal of interest in demonstrating that exciting new capability. Allpress showed that a niobium-oxide-rich composition relative to 1:1 TiO_2:Nb_2O_5 yields disordered regions comprising ordered $Ti_2Nb_{10}O_{29}$ interspersed with ordered $TiNb_2O_7$ in the electron microscope.[59] Coherent boundaries between these structures are compatible with the (3×3) block size of $TiNb_2O_7$ and the (3×4) block size of either polymorph of $Ti_2Nb_{10}O_{29}$ (Figure 2).[59] Note that monoclinic m-$Ti_2Nb_{10}O_{29}$ and orthorhombic o-$Ti_2Nb_{10}O_{29}$ differ only in the long-range sequence of the blocks and that the orthorhombic polymorph is formed only at higher temperatures. Though it is easy to imagine an analogous orthorhombic ordering with (3×3) blocks, the monoclinic phase is the only known $TiNb_2O_7$ polymorph. It is possible for Wadsley defects to order periodically within a host material, leading to a new crystal with a well-defined stoichiometry called an intergrowth phase. Intergrowth compounds have been observed as single crystals in the electron microscope and even in bulk powders in e.g. $Nb_{26}W_4O_{77}$–a 1:1 intergrowth of $Nb_{12}WO_{33}$ and $Nb_{14}W_3O_{44}$.[54,56,59,64] However, only disordered Wadsley defects have been observed in $TiNb_2O_7$ to date.

Owing to the oxygen-vacancy-compensating nature of Wadsley defects, it is believed that point defects are largely absent from crystallographic shear structures.[65,66] The exception to this rule originated with the observations of Reginald Gruehn at Justus Liebig University Giessen that Nb_2O_5-rich block phases containing tunnels of tetrahedra at the corners—and only these phases— showed small, but measurable ranges of stoichiometry.[67] Allpress and Roth also observed varying composition without apparent Wadsley defects at the Nb_2O_5-rich end of the Nb_2O_5–WO_3 phase diagram.[68] These ideas were united under the framework of cation-excess occupation within the

corner tunnels facilitated by cation displacement and a transition from tetrahedral to octahedral coordination,[69] thereby explaining the mystery of the "cation-excess" compound $GeO_2 \cdot 9Nb_2O_5$ that was apparently isostructural with $P_2O_5 \cdot 9Nb_2O_5$ (PNb_9O_{25}).[70,71] The absence of tetrahedral tunnels in $TiNb_2O_7$ and the evidence for Wadsley defect formation suggest a paucity of point defects even if the bulk composition is off-stoichiometric.

$$o\text{-}Ti_2Nb_{10}O_{29} \qquad TiNb_2O_7 \qquad m\text{-}Ti_2Nb_{10}O_{29}$$
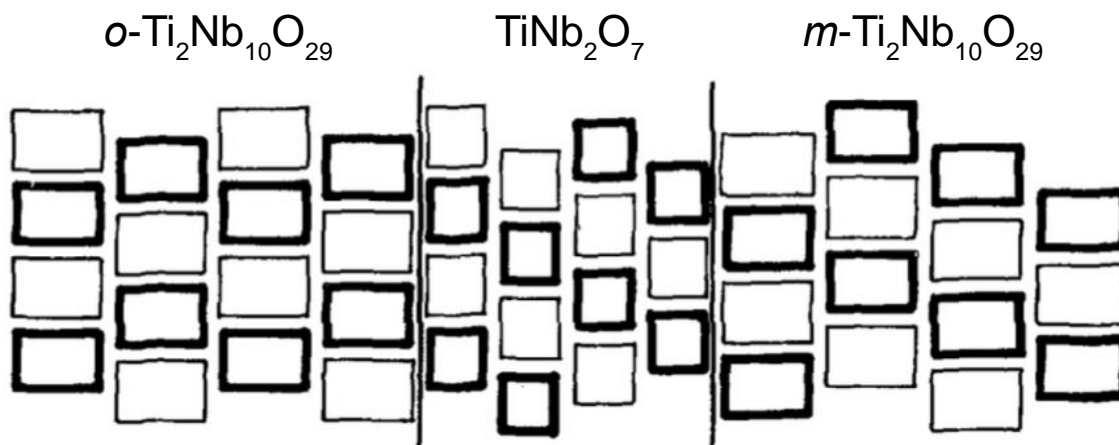
Figure 2. Model of the coherent interface structure between (3 × 4) blocks of octahedra in $Ti_2Nb_{10}O_{29}$ (rectangular) and (3 × 3) blocks of octahedra in $TiNb_2O_7$ (square). Bold outlined blocks and non-bold blocks are offset by ½ of the length a (Ti/Nb)O_6 octahedron in the axis regular to the page. The vertical lines show the positions of Wadsley defects. The prefixes *o-* and *m-* refer to the orthorhombic and monoclinic polymorphs of $Ti_2Nb_{10}O_{29}$, respectively. Reprinted from the *Journal of Solid-state Chemistry*, Vol. 1, J.G. Allpress, "Mixed oxides of Titanium and Niobium: Intergrowth Structures and Defects", pp. 66–81, Copyright 1969, with permission from Elsevier.[59]

In the 1980s, Kamal Forghany, Stuart Anderson, and Tony Cheetham at Oxford and Arne Olsen at the University of Oslo undertook X-ray[72] and electron microscope[73] studies of $TiNb_2O_7$ defect formation under oxygen-poor atmospheres. Two phases are observed initially as oxygen is lost from $TiNb_2O_7$: a niobium-enriched parent phase $Ti^{IV}_{1-x}Nb^{IV}_xNb^V_2O_7$ and a titanium-enriched rutile-phase $Ti^{IV}_{1-y}Nb^{IV}_yO_2$. Upon further reduction, at a certain point the $TiNb_2O_7$ structure cannot accommodate additional niobium enrichment (n.b. Nb_3O_7, i.e. $Nb^{IV}Nb^V_2O_7$, is not a known phase[74]) and it transforms to the orthorhombic $Ti_2Nb_{10}O_{29}$ structure type. The defect transformation mechanism occurs via monoclinic $Ti_2Nb_{10}O_{29}$ regions and a metastable phase $M_{25}O_{60}$ (i.e. $2M_{12}O_{29}+MO_2$) as Nb^{4+} forms at the block edges.[73] The $Ti_2Nb_{10}O_{29}$ can itself be

reduced toward the known $Nb_{12}O_{29}$ phase[23,75] with the simultaneous elimination of rutile $Ti^{IV}_{1-y}Nb^{IV}_yO_2$.

2.3 Cation Ordering. Wadsley proposed a random distribution of titanium and niobium over the five crystallographically distinct cation sites in his original structural model of $TiNb_2O_7$ from single-crystal X-ray diffraction data. In 1973, more than a decade after the host structure of $TiNb_2O_7$ was discovered, Cheetham and Von Dreele from the Inorganic Chemistry Laboratory at the University of Oxford reexamined this question in an early application of Rietveld refinement[76,77] with neutron diffraction data.[78,79] Neutrons are particularly well-suited to differentiate the cations in this system because Ti has a negative neutron scattering length of −3.438 fm while Nb has a positive neutron scattering length of 7.054 fm.[80] From their studies, Cheetham and Von Dreele concluded that there is partial cation ordering with Nb^{5+} exhibiting a strong preference for the central, corner-shared octahedron in the 3×3 block.[78,79] The other four octahedral sites exhibit edge sharing: the corner sites of the block have the most edge sharing and were enriched in lower valent Ti^{4+} while the edge sites of the block, with an intermediate number of shared edges, were slightly enriched in Nb^{5+} relative to a random cation distribution (for details, see Section 3.2.1).[78,79] In 1984, Madeleine Gasperin at Université Pierre-et-Marie-Curie, now part of Sorbonne Université, revisited the question of cation ordering in a single-crystal X-ray diffraction study and obtained virtually identical results (see also Section 3.2.1).[81] We also note that cation ordering was observed at about the same time in a time-of-flight neutron diffraction study by Cheetham and Allen of another Wadsley–Roth phase, $Nb_{14}W_3O_{44}$; in this case, the Nb^{5+} prefers the edge-sharing sites relative to the higher-charged W^{6+}.[82]

2.4 First Electrochemistry. The history of $TiNb_2O_7$ as a lithium-ion battery material originates at Bell Laboratories. In December 1983, Bob Cava (who was formerly a postdoc with Robert Roth), Don Murphy, and Sue Zahurak reported the electrochemical lithiation of $TiNb_2O_7$ to $Li_{2.4}TiNb_2O_7$ when cycled between 3.0 and 1.4 V vs. Li^+/Li.[83] In this seminal publication, the lithiation behavior of a number of other Wadsley–Roth phases were also presented including H-Nb_2O_5, VNb_9O_{25}, $GeNb_{18}O_{47}$, o-$Ti_2Nb_{10}O_{29}$, $TiNb_{24}O_{62}$, $Nb_{12}WO_{33}$, $Nb_{14}W_3O_{44}$, and $Nb_{18}W_8O_{69}$.[4] Simultaneously, in what would become a historical month for high-rate oxide anodes, the Bell labs team along with Tony Santoro at the National Bureau of Standards also published a landmark paper on the lithiation of spinel $Li_4Ti_5O_{12}$ to $Li_7Ti_5O_{12}$.[4] Spinel research charged ahead and $Li_4Ti_5O_{12}$ was developed for commercial applications while, in the rush of new materials being

reported in that period and the long shadow cast by lithium intercalated layered dichalcogenides, $TiNb_2O_7$ disappeared from the battery literature as suddenly as it arrived.

3. Modern Insights: 2010–2020. 3.1 Picking up the Baton. The 30-year period from 1980 to 2010 saw the revolution of lithium-ion batteries all the way from the discovery of $LiCoO_2$[ref.1] to ubiquitous portable electronics and the release of the lithium-ion battery-powered Tesla Roadster. After a nearly 30-year hiatus in the history of $TiNb_2O_7$, John Goodenough's team at the University of Texas at Austin ignited the modern development of $TiNb_2O_7$ as a lithium-ion battery material (Figure 3) with a pair of communications in this journal in 2011.[29,84] In the first report to focus on the battery performance of $TiNb_2O_7$, two modifications were tested: carbon-coating and n-type doping.[29] $TiNb_2O_7$ was prepared from a sol–gel method while d^1 Nb^{4+}-doped $Ti^{IV}_{0.9}Nb^{IV}_{0.1}Nb^V_2O_7$ was prepared with solid-state methods from TiO_2, Nb_2O_5, and Nb metal. Note that the latter compound is analogous to the majority phase observed by reduction of $TiNb_2O_7$ in reducing atmospheres.[72] Carbon-coating was achieved by annealing sucrose-coated particles in argon.[29] Among the new insights on the lithium-ion battery anode characteristics of $TiNb_2O_7$ were the importance of carbon-coating, even with 20% carbon additive in the slurry.[29] Asymmetrical behavior was also observed with delithiation proceeding more rapidly than lithiation. Symmetric half-cell discharge/charge cycling was reported up to 4C/4C while asymmetric cycling up to 2C/~120C was reported (where C, with units of h^{-1}, is a measure of rate; nC corresponds to a current density that would attain n half cycles (charge or discharge) per hour, e.g., 4C would be a 15 minute charge or discharge). The second communication, three months after the first, detailed the first use of $TiNb_2O_7$ in a full lithium-ion battery cell.[84] Spinel $LiNi_{0.5}Mn_{1.5}O_4$ was chosen as the cathode because it led to a 3.0 V full cell. Cathode-limited and anode-limited cells were examined, each with a 1:1.2 capacity ratio. $LiNi_{0.5}Mn_{1.5}O_4$-limited cells exhibited poor capacity retention due to apparent overlithiation of the cathode in the examined voltage window. $TiNb_2O_7$-limited cells, on the other hand, exhibited reasonable capacity retention over the first 50 cycles and utilized about 200 mAh·g^{-1} (based on the mass of $TiNb_2O_7$) when cycled between 3.5 to 1.5 V.[84] Following a provisional patent application to the US Patent Office in July 2010, Goodenough and Jian-Tao Han filed a US patent application titled "Niobium Oxide Compositions and Methods for Using Same" covering $TiNb_2O_7$ on 29 July 2011.[85] The patent was granted on 11 February 2014.[85]
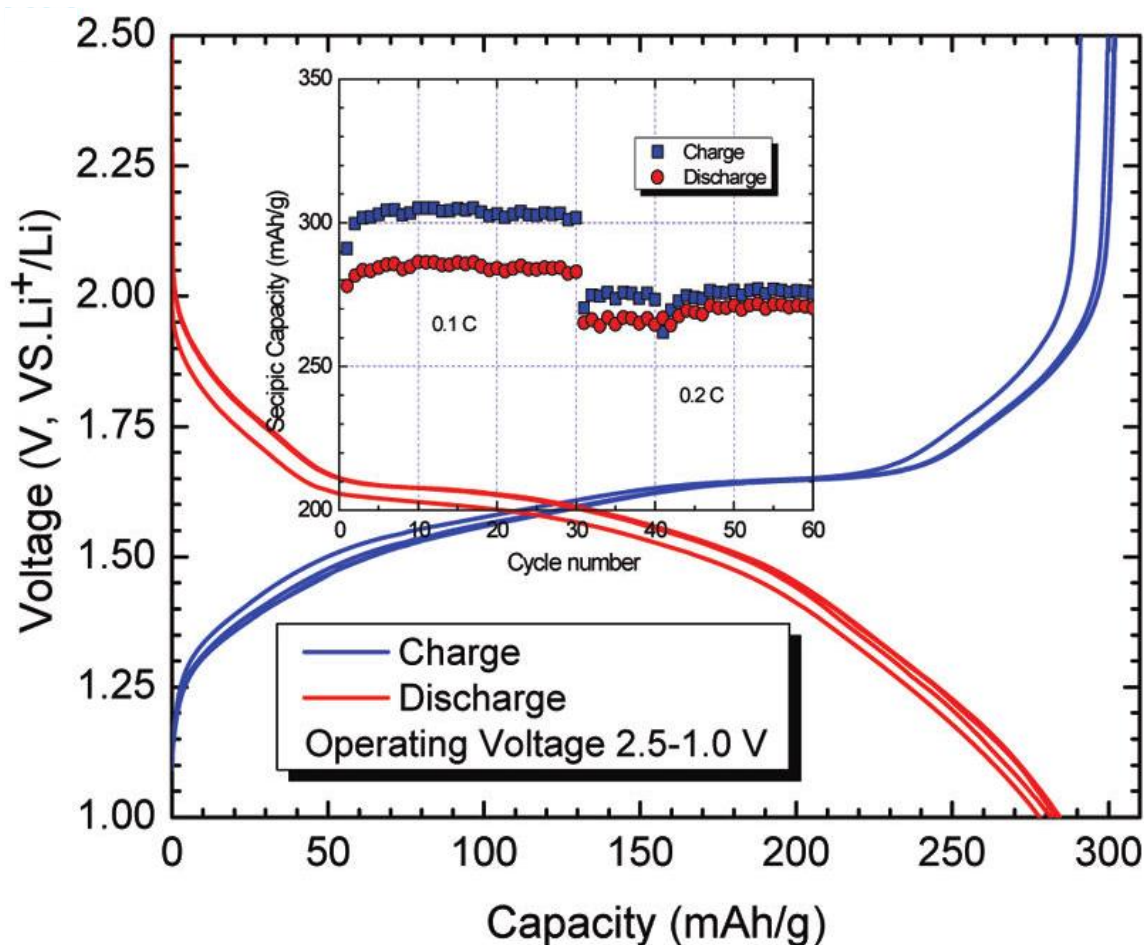
Figure 3. Discharge (red) and charge (blue) curves and cycling performance (inset) of $TiNb_2O_7$ vs. Li first published by Goodenough et al. in 2011. Adapted with permission from J.-T. Han, Y.-H. Huang, J. B. Goodenough, "New Anode Framework", *Chemistry of Materials*, 2011, 23, 2027–2029.[29] Copyright 2011 American Chemical Society.

3.2 Exploring the Details. The renewed interest in $TiNb_2O_7$ has led to the report of various applied studies focused on doping strategies, morphological tuning (size, shape, and porosity of particles), and the construction of composites with various carbon allotropes in an effort to boost performance. A number of studies have also emerged on more fundamental aspects of $TiNb_2O_7$ as an electrode material, including the reaction mechanism, crystal structure, and electronic properties. In order to develop a battery material for commercial applications, its structure–property relationships need to be studied across time-scales and length-scales to understand its

performance and degradation. We will not seek to review comprehensively the publications in this area, but rather provide a modern picture of $TiNb_2O_7$ as a high-rate lithium-ion battery anode.

3.2.1 Crystal Chemistry of $TiNb_2O_7$. Wadsley–Roth phases, including $TiNb_2O_7$, can be pictured as hierarchical structures: atoms assemble into metal oxide octahedra (and sometimes tetrahedra); the octahedra assemble via corner-sharing into ReO_3-like blocks whose size is defined by intersecting crystallographic shear planes; the blocks are then assembled into crystals in a stacking sequence that may or may not require the presence of space-filling tetrahedra. The state-of-the-art picture of $TiNb_2O_7$ comes from a variety of sources including single-crystal X-ray diffreaction,[43,81,33] powder neutron diffraction,[78,79] and density functional theory (DFT) calculations[31]. Wadsley's initial structure model of (3 × 3) blocks of ReO_3-like octahedra joined together by crystallographic shear planes and his space group assignment (*A/2m*, No. 12) have stood the test of time,[43] though other authors have elected to use different space group settings. The five crystallographically distinct cation sites in $TiNb_2O_7$ all occupy octahedra with unique coordination to their neighboring octahedra. First, the octahedra can be broken down into their position within the block: central, edge, and corner. The central site(s) is (are) purely corner sharing with no shared edges in all block structures; there is only one central site in (3 × 3) $TiNb_2O_7$. The two distinct edge sites in $TiNb_2O_7$ differ in that one shares two octahedral edges while the other shares three octahedral edges. Finally, there are also two unique corner sites. Both of these share four octahedral edges; however, they differ in their edge-sharing connectivity as depicted in Figure 4. Comparison of the cation preferential ordering among the various studies is challenging due to the different site numbering schemes and space group settings. Nevertheless, the agreement between the single-crystal XRD and powder neutron data is remarkable, as seen in Table 1 where the sites have been aligned by row normalized to the numbering convention of Cheetham and Von Dreele. The agreement is perhaps more surprising given the differences in sample preparation: Cheetham and Von Dreele measured polycrystalline samples heated to 1350 °C for ~10 days with three intermediate regrindings and rapid cooling;[78,79] Gasperin pulled $TiNb_2O_7$ crystals from a mixture containing TiO_2, Nb_2O_5, barium carbonate, and boric acid that was heated overnight at 1250 °C and then cooled;[81] and Perfler et al. measured crystals slowly cooled from the melt at 1600 °C to 900 °C at 0.5 °C·min^{-1} followed by air quenching[33]. We note that the intensities of the low angle peaks—(100), (10$\bar{2}$), (002) in the face-centered space group setting, e.g., of Cheetham and Von Dreele—are particularly sensitive to the cation ordering. The cation ordering was also

recently studied with DFT calculations in a 30-atom cell (Z = 3). The ground state and three next lowest energy structures contained Ti on the two corner sites labeled M2 by Cheetham and Von Dreele (M5 by Gasperin and Perfler et al.), which shows by far the highest Ti occupancies experimentally, with the third Ti in the cell showing a small preference for an edge or the remaining corner site over the central position.[31] The least energetically favorable cation ordering was found with Ti on the M4 and M5 sites, also in full agreement with experiment.[31]
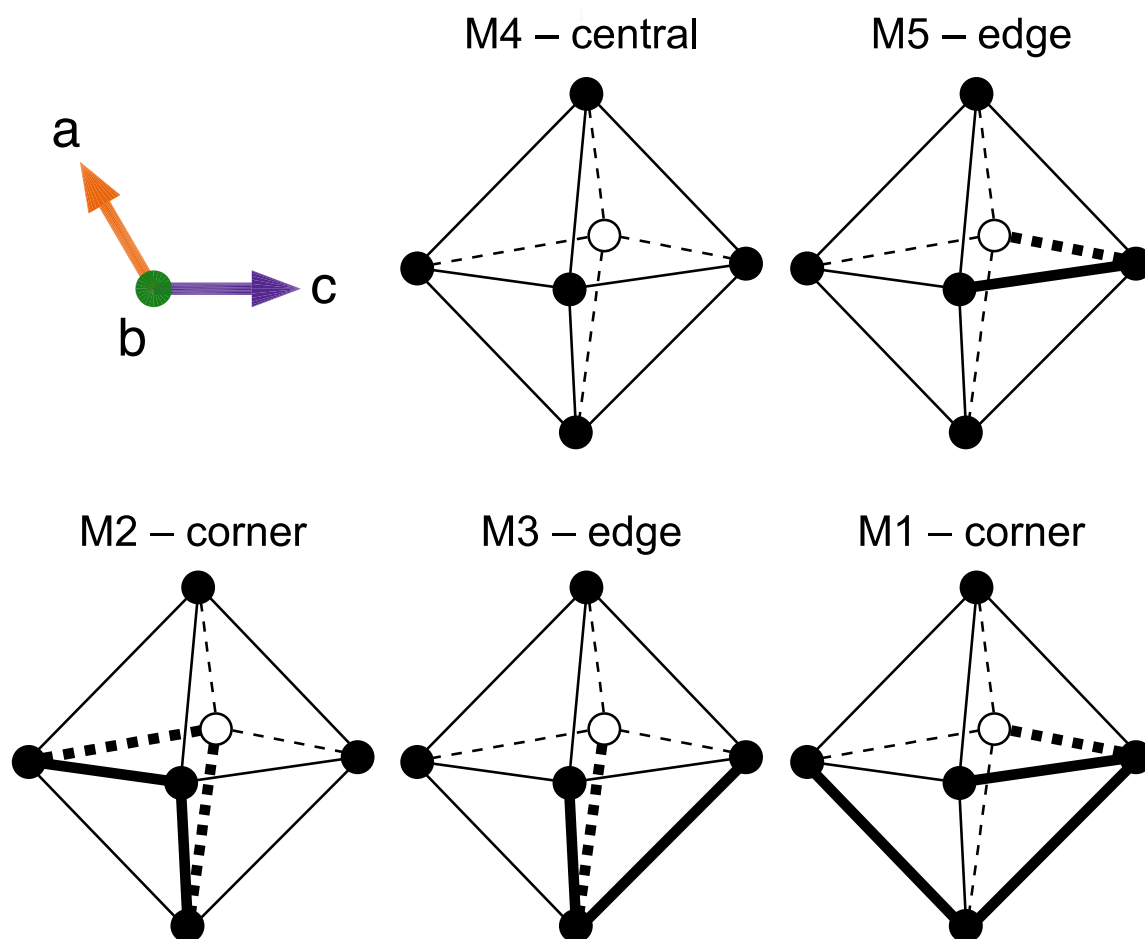
Figure 4. Environment of the five crystallographically distinct (Ti/Nb)O_6 octahedra in TiNb$_2$O$_7$. Bold shading indicates edge-sharing with another octahedra. The labels "central", "edge", and "corner" refer to the position of a given octahedron within the block of ReO$_3$-like octahedra. In TiNb$_2$O$_7$, the two edge-type octahedra differ in number of shared edges and the two corner-type octahedra differ in their coordination to neighboring octahedra. The site numbering scheme follows Cheetham and Von Dreele.[78] See also Figure 1.

Table 1. Ti^{4+}/Nb^{5+} cation site preferences in TiNb$_2$O$_7$.

Model	Cheetham & Von Dreele[78,79]		Gasperin[81]		Perfler et al.[33]	
Block Position[a] [shared oct. edges]	Site	Ti (%)	Site	Ti (%)	Site	Ti (%)
Corner [4 edges]	M1	34(1)	M3	28	M3	35.7(3)
Corner [4 edges]	M2	65(1)	M5	64	M5	62.4(3)
Edge [3 edges]	M3	26(1)	M4	28	M4	27.3(3)
Central [0 edges]	M4	14(2)	M1	19	M1	9.1(5)
Edge [2 edges]	M5	21(1)	M2	19	M2	20.2(3)

[a]See Figures 1 and 4 for a depiction of the positions of each octahedron within the block.
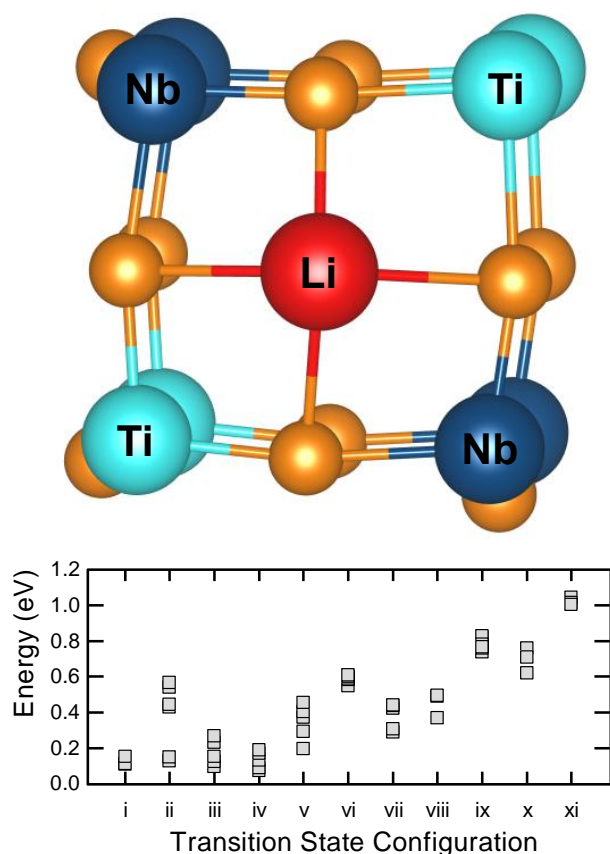
Figure 5. (Top) Atomic picture of a transition state (configuration i) of Li coordinated to four oxygen atoms (orange) in a square tunnel of $TiNb_2O_7$ showing one possible cation configuration of Nb and Ti. (Bottom) Variation in the transition-state energy for different Li hopping transition-state configurations as a function of Ti/Nb ordering. Each square represents a different Ti/Nb ordering. Figure adapted from K. J. Griffith, I. D. Seymour, M. A. Hope, M. M. Butala, L. K. Lamontagne, M. B. Preefer, C. P. Koçer, G. Henkelman, A. J. Morris, M. J. Cliffe, S. E. Dutton, C. P. Grey, "Ionic and Electronic Conduction in $TiNb_2O_7$", *Journal of the American Chemical Society*, 2019, 141, 16706–16725 under CC-BY 4.0 license.[31]

3.2.2 Consequences of Cation Ordering and Defects on Lithium Diffusion.

The defects and cation ordering in $TiNb_2O_7$ are more than historical curiosities; these features play a key role in determining the energetics of lithium diffusion. Lithium traverses $TiNb_2O_7$ through the four parallel *b*-axis tunnels formed by the corner-sharing octahedra within each 3×3 block, hopping between and through four- and five-coordinate sites with low hopping barriers of 100–200 meV.[31] Li can hop between the parallel tunnels just as readily because the pathways between them are also defined by the corner-sharing octahedra in the blocks.[31] The long range 1D diffusion of Li^+ in $TiNb_2O_7$ has been compared to cars traveling down a multi-lane highway; the Li-ions can easily switch lanes, making the transport far less susceptible to diffusion-blocking defects than in single-tunnel 1D conductors such as $LiFePO_4$.[86] It is also interesting to note that several other ReO_3-type structures have been explored for applications as battery electrodes for similar reasons.[46]

That the shear planes exist in two intersecting directions $(CS)^2$ [ref. 64] in $TiNb_2O_7$ is critical to stabilize the structure while facilitating long-range diffusion. Earlier structural studies of the collapse of ReO_3 upon lithium insertion[87] motivated the original exploration of $TiNb_2O_7$ and other Wadsley–Roth phases with intersecting shear planes in 1983.[83] The presence of parallel (i.e. non-intersecting) shear planes $(CS)^1$ is also insufficient to prevent host rearrangement upon lithium insertion and extraction,

regardless of whether these are ordered in ReO_3-derived Magnéli phases, e.g., the homologous series $(Mo,W)_nO_{3n-1}$ or W_nO_{3n-2},[88] or present as disordered Wadsley defects, e.g., WO_{3-x} ($x \lesssim$ 0.04)[89]. Hypothetical three-dimensionally intersecting crystallographic shear planes, i.e. $(CS)^3$, would suppress the diffusion pathways because shear planes effectively prohibit Li-ion transport.[31,90] It is noteworthy that crystallographic shear is not necessarily the only mechanism that can stabilize the ReO_3 framework against the tilts and distortions typical of perovskites. The La^{3+} ions that stabilize the solid electrolyte lithium lanthanum titanium oxide in the perovskite structure can apparently also enable it to reversibly cycle lithium.[91] The role of point defects on ionic transport in these phases has not been studied, but it is a minor consideration since Wadsley defects minimize the occurrence of point defects. On that note, a recent strategy to increase the electronic conductivity of $TiNb_2O_7$[ref.92] and $Ti_2Nb_{10}O_{29}$[ref.93–95] has been to anneal the samples in a reducing atmosphere to introduce d^1 ions Ti^{3+} and/or Nb^{4+} and substantial concentrations of point defects (oxygen vacancies) have been implicated in this process, leading to nominal compositions $TiNb_2O_{6.91}$[ref.92] and $Ti_2Nb_{10}O_{27.1}$[ref.94]. This point defect picture is inconsistent with the available evidence and closer examination would likely reveal a structural origin as previously shown in the 1980s.[72,73] The impact of Ti^{4+}/Nb^{5+} cation ordering is expressed by differences in Li motion activation barriers as a function of the next-nearest-neighbor transition metal occupancy of the transition state configuration (Figure 5).[31]

3.2.3 Structural Evolution during Lithiation. As $TiNb_2O_7$ is lithiated, the host framework evolves through approximately three regions,[96] which are characteristic of Wadsley–Roth phases.[86,97] In various reports, the volume expansion has been determined to be 7.2% to ~$Li_{3.6}TiNb_2O_7$ at 1.0 V (C/8),[96] 6.9% to ~$Li_{3.5}TiNb_2O_7$ at 1.0 V (C/3.3),[98] and 8.4% to ~$Li_{3.33}TiNb_2O_7$ (chemical lithiation)[99]. There is an abrupt color change upon lithiation; the pristine compound is a bright white powder, eventually becoming deep blue toward black at high states of lithiation.[30,31] The color change is associated with n-doping the d^0 $TiNb_2O_7$ and populating the conduction band, pushing the ~2.9–3.1 eV band gap insulator through (partial) localized paramagnetism at low lithium content (up to ~$Li_{1.0}TiNb_2O_7$) toward a metallic lithiated phase at higher lithium concentrations.[30,31] The Ti $3d$ and Nb $4d$ states overlap in energy[31,99] and thus Ti^{4+} and Nb^{5+} are simultaneously reduced[96]. It is believed from X-ray absorption spectroscopy that Nb^{5+} undergoes multielectron reduction to Nb^{3+}.[96,100]

3.2.4 Lithiated TiNb$_2$O$_7$. The structure of highly chemically lithiated Li$_x$TiNb$_2$O$_7$ (x = 2.67, 3.33) has been investigated with high-resolution powder neutron diffraction by Catti et al.[99] Lithiation to Li$_{3.33}$TiNb$_2$O$_7$ causes an anisotropic 8.4% volume expansion driven primarily by a 7.4% expansion along the b-axis. In their refinement, Catti et al. placed the lithium atoms on or very near the mirror plane at (010), i.e. the same height as the metal atoms in the b-axis. These positions are four- or five-coordinated to oxygen atoms, depending on whether they are near a block corner. DFT calculations have provided additional details on the lithium positions,[30,31,99] particularly that the Li site energy minima and the transition states for diffusion are sensitive to Ti/Nb ordering and lithium concentration.[31]

3.2.5 Morphology and Microstructure. The early studies of TiNb$_2$O$_7$ focused on the electrochemical behavior of bulk (µm-scale) particles.[29,30,83] A second wave of nanostructured and porous TiNb$_2$O$_7$ morphologies followed[96,101,102] and now grows steadily. Shorter diffusion distances are expected to increase the rate performance of lithium insertion and extraction. In all electrode materials, the increased particle surface area inherent to nanomaterials must be balanced against other performance factors such as electrode–electrolyte reactivity and cycle life as well as external factors such as cost and scalability (Section 4.1). Gas generation from Li$_4$Ti$_5$O$_{12}$ with standard electrolytes and residual moisture is well-known[103,104] and has now also been found in TiNb$_2$O$_7$-based batteries. Buannic et al. found that TiNb$_2$O$_7$ gassing under reasonable but relatively harsh conditions ((i) cycling against a high voltage LiNi$_{0.5}$Mn$_{1.5}$O$_4$ cathode or (ii) storage at 45 °C against a LiNi$_{1/3}$Mn$_{1/3}$Co$_{1/3}$O$_2$ cathode) was equivalent to, or worse than, Li$_4$Ti$_5$O$_{12}$ and was a function of TiNb$_2$O$_7$ surface area with 32 m$^2 \cdot$g^{-1} particles evolving more gas than 6 m$^2 \cdot$g^{-1} particles annealed at a higher temperature.[105] Wu et al. observed substantial gas formation in cycled TiNb$_2$O$_7$//LiFePO$_4$ pouch cells and a transient SEI layer on TiNb$_2$O$_7$ that formed on lithiation but largely disappeared on delithiation.[106] Future detailed studies of SEI formation on TiNb$_2$O$_7$ are warranted, particularly with respect to its dependence on state-of-charge, crystal facets, and carbon in TiNb$_2$O$_7$–carbon composites.

3.2.6 Substitution and Doping. Doping of TiNb$_2$O$_7$ lithium-ion battery anodes started with Goodenough et al. and the substitution of 10% Nb^{4+} for Ti^{4+}. Since then, cationic dopants such as Ru,[107] Mo,[108] Cu,[109] and anionic doping strategies such as nitridation[110] and oxygen-poor annealing[92] have been examined. Generally, doping is employed to increase the conductivity of the white, electronically insulating TiNb$_2$O$_7$ host and is reported to increase the capacity and rate

performance; however, the electronic conductivity is known to increase by a factor of at least 10^7 upon lithiation[31] (i.e. in situ during battery cycling) so further studies are needed to understand the residual impact of doping on the conductivity after lithiation. This relatively nascent area encompasses a large phase space and there are many outstanding questions. We have already posited that reducing atmospheres likely lead to extended and heterogenous defects like those observed in older electron microscopy studies,[72,73] and not to point defects as presently assumed[92–94]. Furthermore, careful studies of the solid solubility limits and structural implications of other defects are warranted.

4. Commercialization. 4.1 Some Practical Considerations. The landscape for commercial battery materials and methods, constrained by cost and scale considerations, is narrower than for laboratory exploration. Low-cost, sustainable, megaton-scale manufacturing of battery materials is enabled by air-stable, commodity reagents with solid-state or aqueous processing. For example, standard-grade metal oxides, carbonates, and sulfates may be readily used in industry, while metal nitrates and alkoxides are commonly used in research labs but face serious safety and cost barriers to scale-up. Furthermore, the metrics by which performance is measured evolve as a material moves toward practical applications. Crystal, particle, and electrode density reign as gravimetric performance largely yields to volumetric considerations. Particle morphology, electrode loading, electrode calendering (*i.e.* film compaction at mild heat and pressure), active material content, and electrolyte volume must be carefully considered to maximize the energy density while facilitating sufficient ionic and electronic conductivity to meet power and lifetime targets. As with $Li_4Ti_5O_{12}$ and $LiFePO_4$, one generally desires the maximum particle size that meets these performance targets, but some down-scaling and carbon-coating may be necessary. The cost landscape is dynamic and not easy to evaluate when considering a new level of performance, *e.g.*, power densities, charging rates, or non-ambient temperature performance that are fundamentally not safely accessible in graphite-based cells. Lifetime-normalized costs may be significantly different from upfront costs and the (more) relevant value will depend on the application and customer. These are just some of the myriad complex tradeoffs as an electrode candidate moves toward commercialization.

    4.2 Electrode Pairing. Evaluating $TiNb_2O_7$-based cell performance requires pairing this new anode material with a cathode and opens an array of choices and trade-offs. One must consider the

rate-limiting factor, which is typically the graphite electrode and its solid–electrolyte interphase (SEI) for charging rate, first cycle efficiency, and temperature window in a conventional lithium-ion battery. With high-rate oxide anodes such as $TiNb_2O_7$, the cathode may become the limiting factor in some or all of these categories. Another consideration with $TiNb_2O_7$ and similar materials is the relatively high voltage that affords enhanced safety properties to the cell but constricts the cell voltage. The cell energy density is thus a more sensitive function of the cathode voltage when paired with a $TiNb_2O_7$ anode than with a conventional low-voltage anode. Another new parameter to consider when moving from half cells to full cells is the negative-to-positive electrode capacity, or N/P, ratio. Graphite-based cells use an N/P ratio greater than unity, often ~1.1, to ensure that the graphite anode does not overlithiate where it would reach 0 V vs. Li^+/Li and form lithium metal dendrites. On the other hand, Han and Goodenough, in the initially reported $TiNb_2O_7/LiNi_{0.5}Mn_{1.5}O_4$ full cells, showed better cycling performance with an N/P ratio of less than one.

4.3 Toshiba. For their part in the fast-charging anode landscape, and along with a number of other battery manufacturers, Toshiba launched the SCiB™ in 2008 as a safe, long-life, high-power lithium-ion battery employing a lithium titanium oxide anode (LTO) instead of a conventional graphite anode. The latter induces short cycle life and safety issues caused by lithium metal plating on the surface of graphite anode under the conditions of fast-charge, long-term cycles and low-temperature.[111] However, in addition to the lower cell voltage, the theoretical capacity of LTO (175 mAh·g^{-1}) is lower than that of graphite (372 mAh·g^{-1}); energy density should be improved to expand the scope of electrification applications for fast charging anodes. Toshiba, amongst other academic and industrial researchers, has thus continued to pursue enhanced energy density anodes, and several oxides based first on titanium and then on mixtures of titanium and niobium with around 1.5 V operation potential vs. Li^+/Li have been extensively studied.[100,112–114]
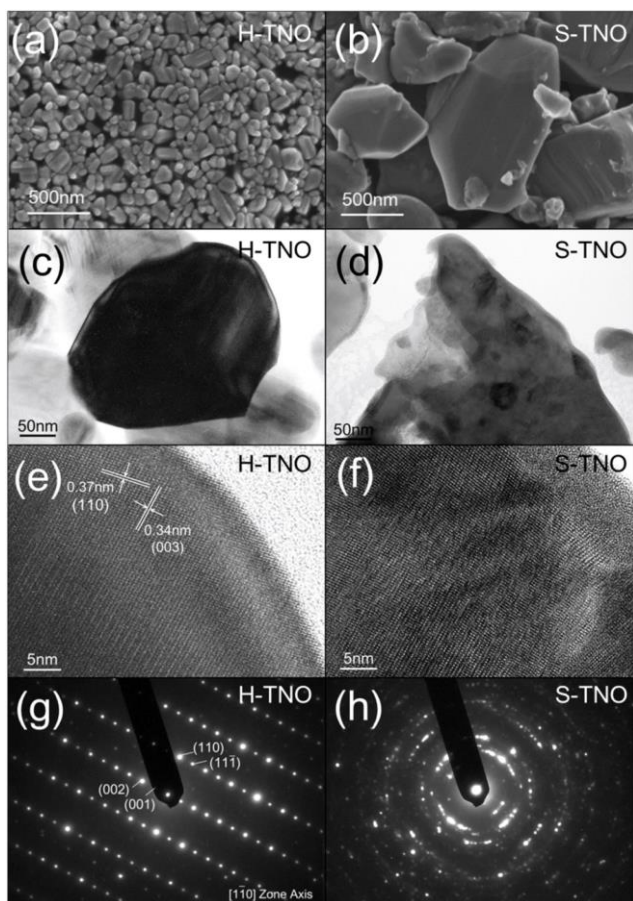
Figure 6. Morphological characterizations of hydrothermally synthesized H-TNO (a), (c), (e), (g) and solid-state-synthesized S-TNO (b), (d), (f), (h) particles by SEM images (a), (b), TEM images (c), (d), (e), (f), and selected area electron diffraction (SAED) patterns (g), (h). Reprinted from *Solid State Ionics*, Vol. 320, K. Ise, S. Morimoto, Y. Harada, N. Takami, "Large Lithium Storage in Highly Crystalline TiNb$_2$O$_7$ Nanoparticles Synthesized by a Hydrothermal Method as Anodes for Lithium-Ion Batteries", pp. 7–15, Copyright 2018, with permission from Elsevier.[100]

4.3.1 Highly Crystallized TiNb$_2$O$_7$.

Toshiba has been developing several titanium niobium oxide related compounds.[100,114] Of the various phases and morphologies, highly crystallized TiNb$_2$O$_7$ (H-TNO) nanoparticles synthesized by a hydrothermal method are reported to show the highest reversible capacity with 341 mAh g^{-1} accessible over a wide potential range of 0.6–3.0 V vs. Li$^+$/Li.[100] The volumetric capacity of H-TNO on the basis of the crystal density of 4.33 g·cm^{-3} is calculated to be 1480 mAh cm^{-3}, which is even higher than that of a graphite anode (837 mAh cm^{-3}). Though Wadsley–Roth complex oxides are commonly cycled to a lower limit of 1.0 V vs. Li$^+$/Li to ensure stability, additional lithium storage in H-TNO is found below this potential. High capacity at high rates in H-TNO is attributed to the short diffusion distances and good lithium diffusivity in the highly crystallized primary particles consisting of a uniform single-crystal face orientation (Figure 6). In internal tests, the reversible capacity, charge-rate capability, and cycle-life performance of H-TNO were significantly higher than those of TNO synthesized by a conventional solid-state reaction route (S-TNO).[100] Toshiba filed a Japanese patent application on 29 October 2010 (JP2010-244658) and, 12 months later, a US patent application covering TNO with highly crystalized particles.[115] The US patent, titled, "Battery active material, nonaqueous electrolyte battery and battery pack," was granted on 6 December 2016.[115] Since 2010, Toshiba has filed more than 90 patent families worldwide for titanium niobium oxide related materials and battery systems.

4.3.2 High-density TNO Composite Electrode. While the laboratory-based work in Section 4.3.1 showed that hydrothermally derived H-TNO exhibits advantages over solid-state-synthesized S-TNO, $NbCl_5$ is a fine chemical and not commercially available in relevant quantities for battery manufacturing. The challenge was then to develop an industrially relevant synthesis method, the result of which was reported to be a highly crystallized TNO compound designated high-density TNO (HD-TNO).[113]

HD-TNO is produced through a modified solid-state method that is more practical in terms of throughput and cost because it avoids extra reagents, fine chemicals, and drying steps. Oxide-
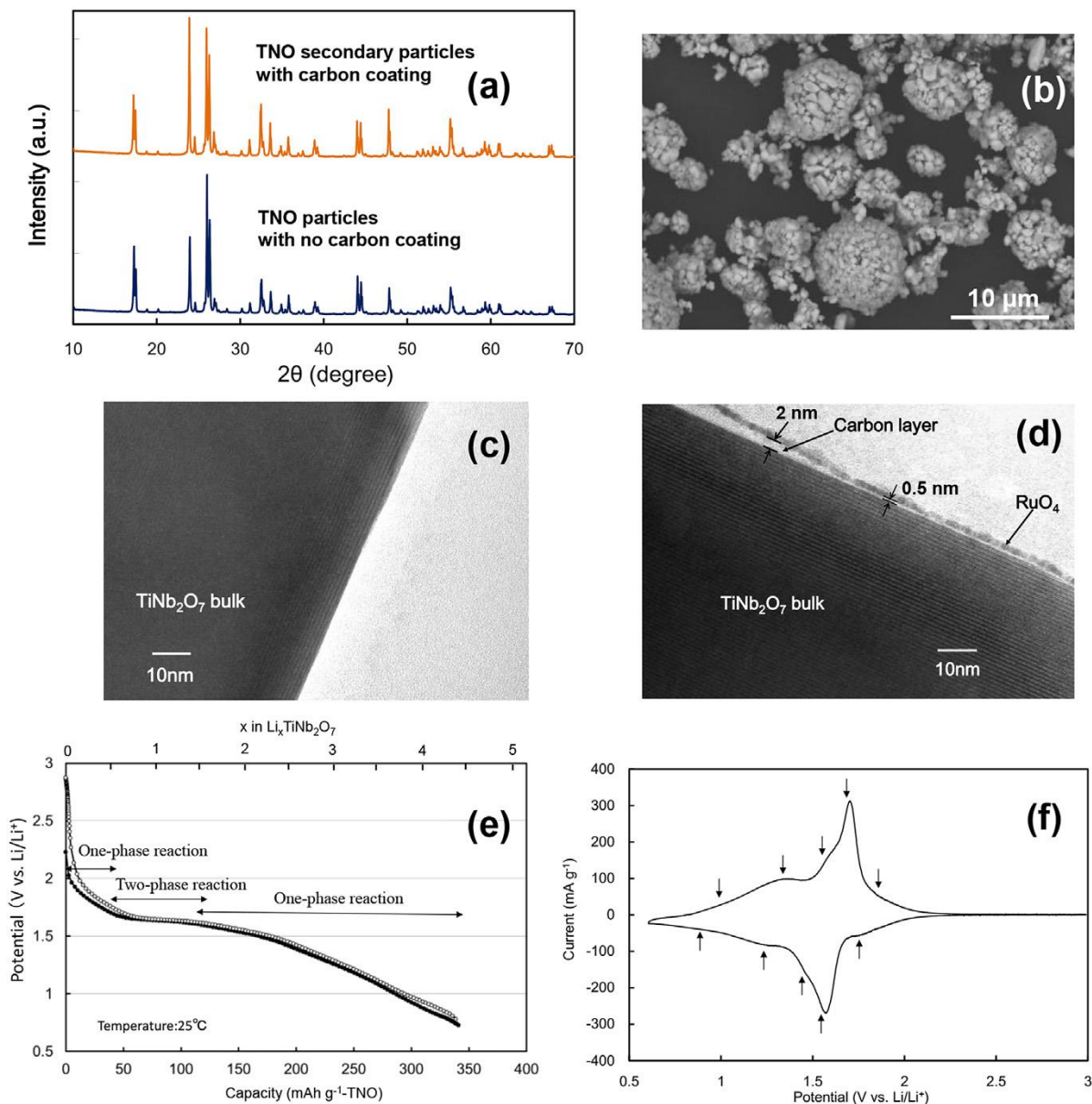
Figure 7. Crystallographic, microstructural, and electrochemical characterization of $TiNb_2O_7$. (a) XRD patterns for TNO secondary particles with carbon coating and primary particles without carbon coating. (b) SEM image for spherical TNO secondary particles. (c–d) TEM images for surface of TNO particle (c) without carbon coating and (d) with carbon coating. The sputtered ruthenium oxide protective layer is visible in (d). (e) Open-circuit plots of HD-TNO electrode during lithium insertion (filled circles) and extraction (open circles) at 15 mA g^{-1}. (f) Cyclic voltammogram of HD-TNO electrode between 0.6 and 3.0 V vs. Li$^+$/Li at a sweep rate of 0.1 mV s^{-1} and the second cycle. Reprinted from the *Journal of Power Sources*, Vol. 396, N. Takami, K. Ise, Y. Harada, T. Iwasaki, T. Kishi, K. Hoshina, "High-Energy, Fast-Charging, Long-Life Lithium-Ion Batteries Using $TiNb_2O_7$ Anodes for Automotive Applications", pp. 429–436, Copyright 2018, with permission from Elsevier. [113]

based precursors such as titanium dioxide and niobium pentahydroxide can be milled together and annealed to produce TNO, which is followed by carbon coating. Recall that a concern for TNO and other titanium–niobium oxides such as $Ti_2Nb_{10}O_{29}$ and $TiNb_{24}O_{62}$ is their poor electronic conductivity. This problem should be especially relevant for practical applications, *i.e.*, thick electrodes and high current densities. As we have already addressed, recent work has shown that the bulk conductivity of $TiNb_2O_7$ increases rapidly on lithiation.[31] However, interparticle electronic conduction[116] remains a critical issue and thus carbon additives and/or particle coatings are currently necessary regardless of the active-material electronic conductivity. This problem has motivated numerous studies of TNO nanoparticle and microsphere composite electrodes containing large quantities of conductive carbon additives such as Ketjen black or acetylene black and low active material mass and volume loadings to enhance the rate capability and cycle life. Even the initial report of Nb(IV)-doped and carbon-coated $TiNb_2O_7$ rate performance noted that 30% carbon additive was required to overcome electronic resistance limitations at high current densities.[29] In another example, TNO composite electrodes consisting of 60 wt% porous TNO nanoparticles, 25 wt% conductive carbon, and 15 wt% binder with a loading of 0.8–2 mg cm^{-2} were reported to obtain a large reversible capacity of 307 mAh g^{-1} based on the TNO active material weight,[117] but the gravimetric capacity of the whole composite electrode is only 184 mAh g^{-1}. Moreover, nanoporous carbons and porous electrode structures lead to a low-density electrode and the volumetric capacity suffers even more than the gravimetric capacity. Both high volumetric energy density and high gravimetric energy density are required for automotive applications. Thus, it is necessary to develop TNO composite electrodes with high density and high active material loading in order to enhance the volumetric energy density at the cell level. To address conductivity issues without sacrificing energy density, Toshiba turned to the spray drying method to produce micrometer-size spherical TNO secondary particles coated with carbon (Figure 7). Sugar-coated TNO was spray dried from an aqueous solution and then annealed in a reducing atmosphere to produce polycrystalline HD-TNO with ~1 μm primary particles, ~10 μm secondary particles, and a ~2 nm conductive carbon coating. HD-TNO is scalable, and it was pursued as a material for high-energy-density electrodes because the powder possesses a high tap density.[113] Also, the amounts of carbon conductor and binder additives can be minimized while still facilitating electron conductive networks. The HD-TNO composite electrode consists of about 90 wt% of the TNO active material and delivers the highest electrode density of reported TNO composite electrodes.[113]

This composite electrode also exhibits high-rate capability, long cycle-life, and a high volumetric capacity of more than twice that of LTO composite anodes.[113]

4.3.3 Large Pouch Battery with TNO. Toshiba produced prototype large-scale TNO//LiNi$_{0.6}$Co$_{0.2}$Mn$_{0.2}$O$_2$ (NCM) pouch batteries with a capacity of 49 Ah in order to evaluate cycle life, fast charge/discharge rate performance and power capability for fully electric and plug-in hybrid vehicle applications.[113] The nominal capacity and nominal voltage at 0.2 C rate were 49 A h and 2.25 V, respectively. The TNO//NCM power cell exhibited an energy density of 350 Wh L^{-1} and 138 Wh kg^{-1}. The volumetric and gravimetric energy densities are considerably lower than state-of-the-art graphite//NCM, but the TNO//NCM power cell is designed to operate under different current density and a range of temperature conditions. The high-rate discharge capability leads to 93% retention of the rated 0.2 C capacity at 10 C (490 A) current through the cell (Figure 8). Non-ambient temperatures are challenging for graphite owing to its sluggish low-temperature
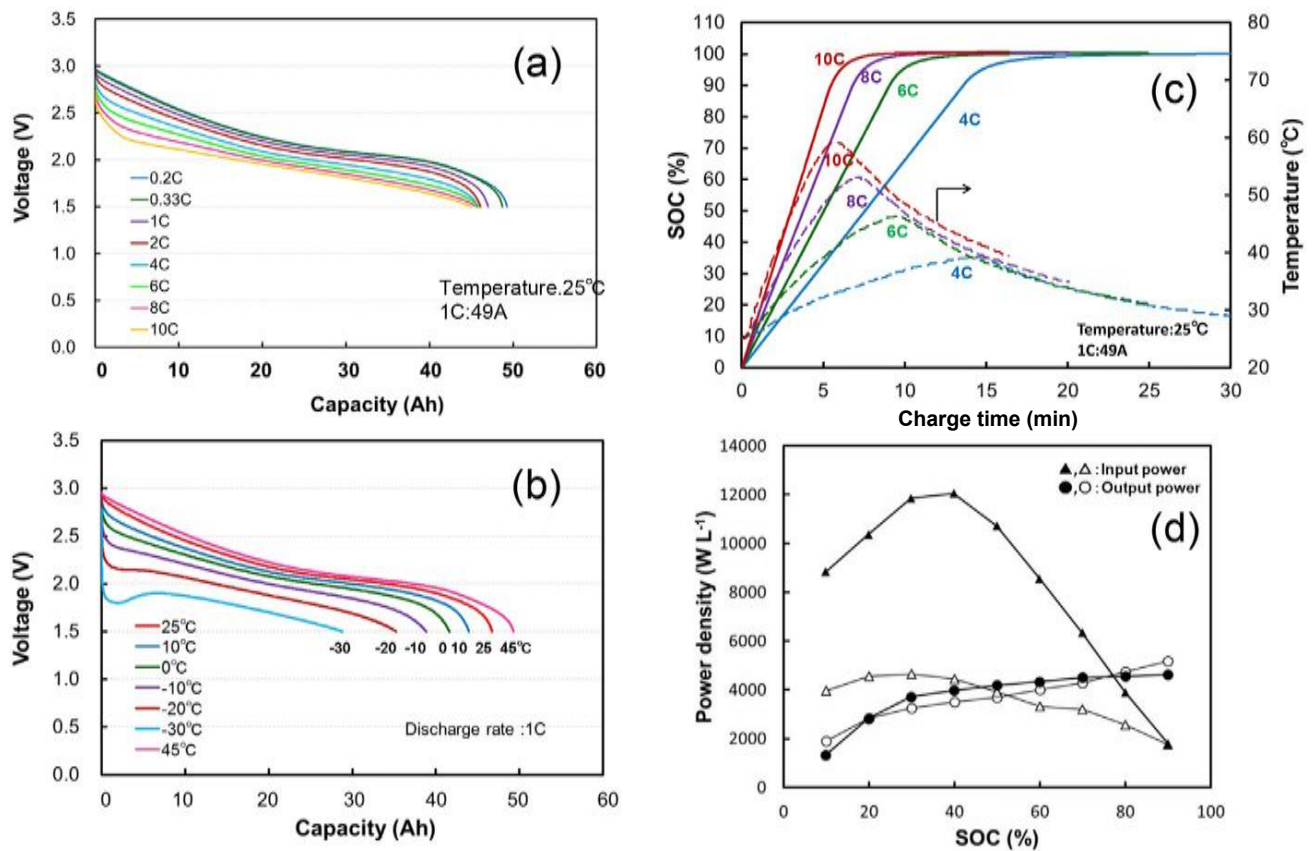
Figure 8. Performance of TNO//NCM batteries. Discharge voltage curves at various (a) discharge rates and (b) temperatures. (c) Changes in state-of-charge (SOC, solid line) and battery temperature (dashed line) at various charge rates. (d) Input (triangles) and output (circles) power density of the TNO//NCM battery (filled shapes) and LTO//NCM battery (open shapes) for 10 s current pulses as a function of SOC. Reprinted from the *Journal of Power Sources*, Vol. 396, N. Takami, K. Ise, Y. Harada, T. Iwasaki, T. Kishi, K. Hoshina, "High-Energy, Fast-Charging, Long-Life Lithium-Ion Batteries Using TiNb$_2$O$_7$ Anodes for Automotive Applications", pp. 429–436, Copyright 2018, with permission from Elsevier.[113]

diffusion and fragile SEI. Meanwhile, the TNO//NCM cell also demonstrates a 63% capacity retention at −30 °C, relative to ambient temperature. The recharging time from 0 to 90% SOC at 10 C rate at 25 °C is 5.5 min and the maximum temperature at the cell surface is 59 °C. It may be necessary to cool down the batteries during ultrafast charging, but mild cooling is a practical option. At the opposite extreme of cell surface temperatures, the battery can be recharged over the same SOC range in 12 min at −10 °C with neither accelerated degradation nor lithium metal plating. A nail penetration test was also carried out to evaluate the safety properties of this 49 Ah TNO//NCM pouch cell in its fully charged state. The variations of cell voltage, cell temperature at various locations, nail temperature, and atmosphere temperature after nail penetration are shown (Figure 9). After nail penetration, the voltage gradually decreased to 1.0 V over 100 minutes, and the cell temperature rose to a maximum value of 48 °C at the center. The TNO anode has higher thermal stability than carbonaceous materials such as graphite[118] and an almost insulative character except for the very thin carbon coating on its surface, which is expected to burn off at the internal short-circuit point. Thus, the use of a TNO anode – like LTO – appears to be an effective method to prevent thermal runaway. The maximum output-power and input-power density at 50% SOC are 4 kW L^{-1} and 10 kW L^{-1}, respectively. Interestingly, the input power density is much higher than the output, which would be suitable for a regenerative braking system in order to recover kinetic energy as efficiently as possible.

Figure 9. Nail-penetration test of 49 Ah TNO//NCM pouch-cell battery. The nail penetration occurs at time = 0 min. Voltage, nail temperature, cell temperature and atmosphere temperature are measured before and after the nail penetration. The schematic shows the nine cell temperature sensor locations, color coded to the temperature curves.

4.4 Bringing a New Element to the Market. Reported lithium-ion battery material candidates cover nearly the entire periodic table. On the other hand, only a few elements are used in bulk in commercial materials; the raw material metals conversation typically focuses on Li, Al, and the first-row transition metals Ti, Mn, Fe, Co, Ni, and Cu. It is reasonable then to wonder whether a new element, particularly a $4d$ transition metal, can be adopted and whether the supply chain exists at the scale relevant to the modern lithium-ion battery market. The annual production of niobium in 2019 was about 74,000 tons, primarily as ferroniobium alloy used for high-strength steel applications, whereas the $Li_4Ti_5O_{12}$ market currently stands at an estimated 3000 tons.[21,25,26] In 2018, Toshiba Corporation partnered with CBMM, a niobium producer, to develop and manufacture $TiNb_2O_7$ at the pilot-scale manufacturing facility in Kashiwazaki, Japan.[119] Together, the companies are working to provide battery cells and modules based on the TNO anode technology. Considering that niobium is a critical element, like other battery components including lithium, cobalt, manganese, graphite, titanium, and to a lesser extent, nickel,[25,27,28] supply partnerships are important. This may be particularly true for resources such as niobium that have few suppliers. There is a recent trend among large-scale battery cell manufacturers such as LG Chem and electric vehicle companies such as BMW and Tesla to announce or ask for such partnerships in the nickel and cobalt markets.[120–122] Along similar lines, electrode powders generally require battery-grade precursors that may differ from those for other technical or metallurgical applications, and this is also a factor to consider for niobium.

5. Looking to the Future: Beyond 2020. 5.1 TNO. The example of TNO demonstrates that a promising battery material, which itself may be the product of years or decades of research is only the beginning. Manufacturing scale-up also requires a sustained effort and potentially supply chain development. The progress of TNO from its "rediscovery" in 2011 until now is an indication that opportunities exist for truly new chemistries in the commercial battery sector. Many hurdles have to be crossed to reach industrial production, but this can occur in a relatively short timeframe and is accelerated by a bedrock of fundamental academic studies. Moving forward, market development initiatives are being carried out to assess the myriad possible applications ranging from electric and hybrid family vehicles, heavy-duty trucks, buses, and trains to grid-scale energy storage systems to power-hungry devices such as cordless tools, forklifts, drones, and robots. The

vision is for TNO not just to be an energy-dense alternative to LTO but to be an enabling energy storage technology.

5.2 NWO. $TiNb_2O_7$ is one of a family of niobium-based Wadsley–Roth structures. Among the diversity of chemistries, some of the most recent results of some of the authors have shown that larger block phases such as $Nb_{16}W_5O_{55}$ with 4×5 blocks and $Nb_{18}W_8O_{69}$ with 5×5 blocks (NWO phases) offer a few additional exciting features such as (i) multielectron redox of W^{6+} to W^{4+}, (ii) excellent electronic properties owing to the lack of electron-localizing Ti centers, and (iii) a higher density of central tunnels that accommodate faster diffusion than the edge sites adjacent to shear planes.[86,90,123,124] These features have led to high-rate performance without stringent carbon-coating and particle size or morphology requirements. Just as the Wadsley–Roth crystallographic shear structures began with $TiNb_2O_7$, we hope that this work will lead to the next generation of advanced batteries related to TNO.

Notes: The authors declare the following competing financial interest(s): K.J.G. and C.P.G. are major shareholders in CB2tech Limited, a start-up company developing fast charging batteries based on high-rate anode materials. Y.H. and S.E. are employees of Toshiba Corporation, which is commercializing TNO. R.M.R. and R.S.M. are employees of CBMM that is a niobium producer and a partner in the commercialization of TNO. J.B.G holds a US patent related to TNO anodes for lithium-ion batteries.

References
(1)   Mizushima, K.; Jones, P. C.; Wiseman, P. J.; Goodenough, J. B. Li_xCoO_2 ($0<x\leq1$): A New Cathode Material for Batteries of High Energy Density. *Mater. Res. Bull.* **1980**, *15*, 783–789.
(2)   Padhi, A. K.; Nanjundaswamy, K. S.; Goodenough, J. B. Phospho-olivines as Positive-Electrode Materials for Rechargeable Lithium Batteries. *J. Electrochem. Soc.* **1997**, *144* (4), 1188–1194. https://doi.org/10.1149/1.1837571.

(3)   Thackeray, M. M.; David, W. I. F.; Bruce, P. G.; Goodenough, J. B. Lithium Insertion into Manganese Spinels. *Mater. Res. Bull.* **1983**, *18* (4), 461–472. https://doi.org/10.1016/0025-5408(83)90138-1.

(4)   Murphy, D. W.; Cava, R. J.; Zahurak, S. M.; Santoro, A. Ternary Li_xTiO_2 Phases from Insertion Reactions. *Solid State Ion.* **1983**, *9*, 413–417. https://doi.org/10.1016/0167-2738(83)90268-0.

(5)   Marginedes, D. Commercial Developments of LMP Technology in Mobility and Stationary Domains; Ft. Lauderdale, FL, USA, 2019.

(6)   Thackeray, M. *Running with Lithium—Empowering the Earth: A Personal Journey*; Archway Publishing, 2019.

(7)   Press release: The Nobel Prize in Chemistry 2019 https://www.nobelprize.org/prizes/chemistry/2019/press-release (accessed May 07, 2020).

(8)   Scientific Background: Lithium-ion batteries https://www.nobelprize.org/prizes/chemistry/2019/advanced-information (accessed May 07, 2020).

(9)   Brédas, J.-L.; Buriak, J. M.; Caruso, F.; Choi, K.-S.; Korgel, B. A.; Palacín, M. R.; Persson, K.; Reichmanis, E.; Schüth, F.; Seshadri, R.; Ward, M. D. An Electrifying Choice for the 2019 Chemistry Nobel Prize: Goodenough, Whittingham, and Yoshino. *Chem. Mater.* **2019**, *31* (21), 8577–8581. https://doi.org/10.1021/acs.chemmater.9b04345.

(10)   Goodenough, J. B. Evolution of Strategies for Modern Rechargeable Batteries. *Acc. Chem. Res.* **2013**, *46* (5), 1053–1061. https://doi.org/10.1021/ar2002705.

(11)   Goodenough, J. B. Changing Outlook for Rechargeable Batteries. *ACS Catal.* **2017**, *7* (2), 1132–1135. https://doi.org/10.1021/acscatal.6b03110.

(12)   Goodenough, J. B. Personal Journey into Solid State Chemistry. *J. Solid State Chem.* **2019**, *271*, 387–392. https://doi.org/10.1016/j.jssc.2018.12.019.

(13)   Scrosati, B. History of Lithium Batteries. *J. Solid State Electrochem.* **2011**, *15* (7–8), 1623–1630. https://doi.org/10.1007/s10008-011-1386-8.

(14)   *Lithium Batteries: Science and Technology*, First softcover printing.; Nazri, G.-A., Pistoia, G., Eds.; Springer: New York, NY, 2009.

(15)   LeVine, S. *The Powerhouse: Inside the Invention of a Battery to Save the World*; VIKING: New York, 2015.

(16)   Reddy, M. V.; Mauger, A.; Julien, C. M.; Paolella, A.; Zaghib, K. Brief History of Early Lithium-Battery Development. *Materials* **2020**, *13* (8), 1884. https://doi.org/10.3390/ma13081884.

(17)   Blomgren, G. E. The Development and Future of Lithium Ion Batteries. *J. Electrochem. Soc.* **2017**, *164* (1), A5019–A5025. https://doi.org/10.1149/2.0251701jes.

(18)   Placke, T.; Kloepsch, R.; Dühnen, S.; Winter, M. Lithium Ion, Lithium Metal, and Alternative Rechargeable Battery Technologies: The Odyssey for High Energy Density. *J. Solid State Electrochem.* **2017**, *21* (7), 1939–1964. https://doi.org/10.1007/s10008-017-3610-7.

(19)   Whittingham, M. S. History, Evolution, and Future Status of Energy Storage. *Proc. IEEE* **2012**, *100*, 1518–1534. https://doi.org/10.1109/JPROC.2012.2190170.

(20)   Toshiba Rechargeable Battery SCiB https://www.scib.jp/en/download/ToshibaRechargeableBattery-en.pdf.

(21)   Pillot, C. *The Rechargeable Battery Market*; 28th edition; Avicenne Energy: Paris, France, 2020.

(22) Elmaslmane, A. R.; Watkins, M. B.; McKenna, K. P. First-Principles Modeling of Polaron Formation in TiO_2 Polymorphs. *J. Chem. Theory Comput.* **2018**, *14* (7), 3740–3751. https://doi.org/10.1021/acs.jctc.8b00199.

(23) Cava, R. J.; Batlogg, B.; Krajewski, J. J.; Gammel, P.; Poulsen, H. F.; Peck, W. F.; Rupp, L. W. Antiferromagnetism and Metallic Conductivity in $Nb_{12}O_{29}$. *Nature* **1991**, *350* (6319), 598–600. https://doi.org/10.1038/350598a0.

(24) Hu, Z.; Gao, S. Upper Crustal Abundances of Trace Elements: A Revision and Update. *Chem. Geol.* **2008**, *253* (3–4), 205–221. https://doi.org/10.1016/j.chemgeo.2008.05.010.

(25) Schulz, K. J.; Piatak, N. M.; Papp, J. F. Niobium and tantalum, Chap. M of Schulz, K. J.; DeYoung, J. H., Jr.; Seal, R.R., II; Bradley, D. C., eds., Critical Mineral Resources of the United States—Economic and Environmental Geology and Prospects for Future Supply: U.S. Geological Survey Professional Paper 1802, 2017, M1–M34. https://doi.org/10.3133/pp1802M.

(26) *Minerals Yearbook*; United States Geological Survey, 2019; Vol. 1. Metals and Minerals.

(27) Erdmann, L.; Graedel, T. E. Criticality of Non-Fuel Minerals: A Review of Major Approaches and Analyses. *Environ. Sci. Technol.* **2011**, *45* (18), 7620–7630. https://doi.org/10.1021/es200563g.

(28) Petty, T. R. Final List of Critical Minerals 2018. *Fed. Regist.* **2018**, *83* (97), 23295–23296.

(29) Han, J.-T.; Huang, Y.-H.; Goodenough, J. B. New Anode Framework for Rechargeable Lithium Batteries. *Chem. Mater.* **2011**, *23* (8), 2027–2029. https://doi.org/10.1021/cm200441h.

(30) Lu, X.; Jian, Z.; Fang, Z.; Gu, L.; Hu, Y.-S.; Chen, W.; Wang, Z.; Chen, L. Atomic-Scale Investigation on Lithium Storage Mechanism in $TiNb_2O_7$. *Energy Environ. Sci.* **2011**, *4* (8), 2638–2644. https://doi.org/10.1039/C0EE00808G.

(31) Griffith, K. J.; Seymour, I. D.; Hope, M. A.; Butala, M. M.; Lamontagne, L. K.; Preefer, M. B.; Koçer, C. P.; Henkelman, G.; Morris, A. J.; Cliffe, M. J.; Dutton, S. E.; Grey, C. P. Ionic and Electronic Conduction in $TiNb_2O_7$. *J. Am. Chem. Soc.* **2019**, *141*, 16706−16725. https://doi.org/10.1021/jacs.9b06669.

(32) Dolotko, O.; Senyshyn, A.; Mühlbauer, M. J.; Boysen, H.; Monchak, M.; Ehrenberg, H. Neutron Diffraction Study of $Li_4Ti_5O_{12}$ at Low Temperatures. *Solid State Sci.* **2014**, *36*, 101–106. https://doi.org/10.1016/j.solidstatesciences.2014.08.002.

(33) Perfler, L.; Kahlenberg, V.; Wikete, C.; Schmidmair, D.; Tribus, M.; Kaindl, R. Nanoindentation, High-Temperature Behavior, and Crystallographic/Spectroscopic Characterization of the High-Refractive-Index Materials $TiTa_2O_7$ and $TiNb_2O_7$. *Inorg. Chem.* **2015**, *54* (14), 6836–6848. https://doi.org/10.1021/acs.inorgchem.5b00733.

(34) Hull, A. W. A New Method of X-Ray Crystal Analysis. *Phys. Rev.* **1917**, *10* (6), 661–696. https://doi.org/10.1103/PhysRev.10.661.

(35) E. A. Durbin; C. G. Harman. *An Appraisal of the Sintering Behavior and Thermal Expansion of Some Columbites*; BMI-791; Battelle Memorial Institute, 1952; p 14.

(36) E. A. Durbin; H. E. Wagner; C. G. Harman. *Properties of Some Columbium Oxide-Basis Ceramics*; BMI-792; Battelle Memorial Institute, 1952; p 15.

(37) Roth, R. S.; Coughanour, L. W. Phase Equilibrium Relations in the Systems Titania-Niobia and Zirconia-Niobia. *J. Res. Natl. Bur. Stand.* **1955**, *55* (4), 209–213. https://doi.org/10.6028/jres.055.023.

(38) Wadsley, A. D. Mixed Oxides of Titanium and Niobium. II. The Crystal Structures of the Dimorphic Forms $Ti_2Nb_{10}O_{29}$. *Acta Crystallogr.* **1961**, *14* (6), 664–670. https://doi.org/10.1107/S0365110X6100200X.

(39) Roth, R. S.; Wadsley, A. D. Mixed Oxides of Titanium and Niobium: The Crystal Structure of $TiNb_{24}O_{62}$ ($TiO_2 \cdot 12Nb_2O_5$). *Acta Crystallogr.* **1965**, *18* (4), 724–730. https://doi.org/10.1107/S0365110X65001664.

(40) Roth, R. S.; Wadsley, A. D.; Gatehouse, B. M. Composition of the Phases in the Systems $NbO_2 - Nb_2O_5$ and $TiO_2 - Nb_2O_5$. *Naturwissenschaften* **1964**, *51* (11), 262–263.

(41) Roth, R. S. Thermal Stability of Long Range Order in Oxides. *Prog. Solid State Chem.* **1980**, *13* (2), 159–192. https://doi.org/10.1016/0079-6786(80)90003-5.

(42) Griffith, K. J.; Senyshyn, A.; Grey, C. P. Structural Stability from Crystallographic Shear in $TiO_2 - Nb_2O_5$ Phases: Cation Ordering and Lithiation Behavior of $TiNb_{24}O_{62}$. *Inorg. Chem.* **2017**, *56* (7), 4002–4010. https://doi.org/10.1021/acs.inorgchem.6b03154.

(43) Wadsley, A. D. Mixed Oxides of Titanium and Niobium. I. *Acta Crystallogr.* **1961**, *14* (6), 660–664. https://doi.org/10.1107/S0365110X61001996.

(44) Wadsley, A. D. Modern Structural Inorganic Chemistry. *J. Proc. R. Soc. New South Wales* **1958**, *92*, 25–35.

(45) Andersson, S.; Wadsley, A. D. Crystallographic Shear and Diffusion Paths in Certain Higher Oxides of Niobium, Tungsten, Molybdenum and Titanium. *Nature* **1966**, *211* (5049), 581–583. https://doi.org/10.1038/211581a0.

(46) Evans, H. A.; Wu, Y.; Seshadri, R.; Cheetham, A. K. Perovskite-Related ReO_3-Type Structures. *Nat. Rev. Mater.* **2020**, *5* (3), 196–213. https://doi.org/10.1038/s41578-019-0160-x.

(47) Wadsley, A. D. The Crystal Chemistry of Non-Stoichiometric Compounds. *Revs Pure Appl Chem* **1955**, *5*, 165–193.

(48) Gatehouse, B. M.; Wadsley, A. D. The Crystal Structure of the High Temperature Form of Niobium Pentoxide. *Acta Crystallogr.* **1964**, *17* (12), 1545–1554. https://doi.org/10.1107/S0365110X6400384X.

(49) Roth, R. S.; Wadsley, A. D.; Andersson, S. The Crystal Structure of PNb_9O_{25}, ($P_2O_5 \cdot Nb_2O_5$). *Acta Crystallogr.* **1965**, *18* (4), 643–647. https://doi.org/10.1107/S0365110X65001500.

(50) Roth, R. S.; Wadsley, A. D. Multiple Phase Formation in the Binary System $Nb_2O_5 - WO_3$. I. Preparation and Identification of Phases. *Acta Crystallogr.* **1965**, *19* (1), 26–32. https://doi.org/10.1107/S0365110X65002712.

(51) Roth, R. S.; Wadsley, A. D. Multiple Phase Formation in the Binary System $Nb_2O_5 - WO_3$. II. The Structure of the Monoclinic Phases $WNb_{12}O_{33}$ and $W_5Nb_{16}O_{55}$. *Acta Crystallogr.* **1965**, *19* (1), 32–38. https://doi.org/10.1107/S0365110X65002724.

(52) Roth, R. S.; Wadsley, A. D. Multiple Phase Formation in the Binary System $Nb_2O_5 - WO_3$. III. The Structures of the Tetragonal Phases $W_3Nb_{14}O_{44}$ and $W_8Nb_{18}O_{69}$. *Acta Crystallogr.* **1965**, *19* (1), 38–42. https://doi.org/10.1107/S0365110X65002736.

(53) Roth, R. S.; Wadsley, A. D. Multiple Phase Formation in the Binary System $Nb_2O_5 - WO_3$. IV. The Block Principle. *Acta Crystallogr.* **1965**, *19* (1), 42–47. https://doi.org/10.1107/S0365110X65002748.

(54) Andersson, S.; Mumme, W. G.; Wadsley, A. D. Multiple Phase Formation in the Binary System $Nb_2O_5 - WO_3$. V. The Structure of $W_4Nb_{26}O_{77}$, an Ordered Intergrowth of the

Adjoining Compounds $WNb_{12}O_{33}$ and $W_3Nb_{14}O_{44}$. *Acta Crystallogr.* **1966**, *21* (5), 802–808. https://doi.org/10.1107/S0365110X66003852.

(55) Allpress, J. G.; Sanders, J. V.; Wadsley, A. D. Multiple Phase Formation in the Binary System Nb_2O_5–WO_3. VI. Electron Microscopic Observation and Evaluation of Non-Periodic Shear Structures. *Acta Crystallogr. B* **1969**, *25* (6), 1156–1164. https://doi.org/10.1107/S0567740869003669.

(56) Allpress, J. G.; Wadsley, A. D. Multiple Phase Formation in the Binary System Nb_2O_5–WO_3: VII. Intergrowth of H-Nb_2O_5 and $WNb_{12}O_{33}$. *J. Solid State Chem.* **1969**, *1* (1), 28–38. https://doi.org/10.1016/0022-4596(69)90005-X.

(57) A. K. Cheetham. Structural Studies on Nonstoichiometric Oxides Using X-Ray and Neutron Diffraction. In *Nonstoichiometric Oxides*; O. Toft Sørensen, Ed.; Materials Science Series; Academic Press: London, 1981; pp 399–433.

(58) Wadsley, A. D.; Andersson, S. Crystallographic Shear, and the Niobium Oxides and Oxide Fluorides in the Composition Region MX_x, $2.4 < x < 2.7$. In *Perspectives in Structural Chemistry*; Dunitz, J. D., Ibers, J. A., Eds.; John Wiley & Sons, Inc., 1970; Vol. III, pp 1–58.

(59) Allpress, J. G. Mixed Oxides of Titanium and Niobium: Intergrowth Structures and Defects. *J. Solid State Chem.* **1969**, *1* (1), 66–81. https://doi.org/10.1016/0022-4596(69)90010-3.

(60) *Solid State Chemistry*; Roth, R. S., Schneider, Jr., S. J., Eds.; Special Publication; National Bureau of Standards (U.S.), 1972.

(61) Wadsley, A. D. Nonstoichiometric Metal Oxides. In *Nonstoichiometric Compounds*; Advances in Chemistry; American Chemical Society, 1963; Vol. 39, pp 23–36. https://doi.org/10.1021/ba-1964-0039.ch002.

(62) Andersson, S. Arthur David Wadsley 1918 – 1969. *J. Solid State Chem.* **1970**, *1* (3–4), iv–vi. https://doi.org/10.1016/0022-4596(70)90107-6.

(63) *The Chemistry of Extended Defects in Non-Metallic Solids*; Eyring, L., O'Keeffe, M., Eds.; North-Holland: Amsterdam, 1970.

(64) Eyring, L.; Tai, L.-T. The Structural Chemistry of Some Complex Oxides: Ordered and Disordered Extended Defects. In *Crystalline and Noncrystalline Solids*; Hannay, N. B., Ed.; Treatise on Solid State Chemistry; Plenum Press: New York, NY, 1976; Vol. 3, pp 167–252.

(65) A. D. Wadsley. Crystallographic Shear and Planar Faults in Solids. In *Proceedings of the 6th International Symposium on the Reactivity of Solids*; Wiley-Interscience: Schenectady, New York, 1969; pp 1–15.

(66) LeRoy Eyring. Structure, Defects, and Nonstoichiometry in Oxides: An Electron Microscope View. In *Nonstoichiometric Oxides*; O. Toft Sørensen, Ed.; Materials Science Series; Academic Press: London, 1981; pp 337–398.

(67) Reginald Gruehn. Some Aspects of the Investigation of Intergrowth Phases in Nb_2O_5-Rich Systems. In *Solid State Chemistry*; Robert S. Roth, Schneider, Jr., S. J., Eds.; National Bureau of Standards Special Publication; U. S. Government Printing Office: Washington D.C., 1972; pp 63–86.

(68) Allpress, J. G.; Roth, R. S. The Effect of Annealing on the Concentration of Wadsley Defects in the Nb_2O_5–WO_3 System. *J. Solid State Chem.* **1971**, *3* (2), 209–216. https://doi.org/10.1016/0022-4596(71)90030-2.

(69) Anderson, J. S.; Browne, J. M.; Cheetham, A. K.; Von Dreele, R. B.; Hutchison, J. L.; Lincoln, F. J.; Bevan, D. J. M.; Straehle, J. Point Defects and Extended Defects in Niobium Oxides. *Nature* **1973**, *243*, 81–83.

(70) Anderson, J. S.; Bevan, D. J. M.; Cheetham, A. K.; Dreele, R. B. V.; Hutchison, J. L.; Strahle, J. The Structure of Germanium Niobium Oxide, an Inherently Non-Stoichiometric "Block" Structure. *Proc. R. Soc. Lond. Math. Phys. Eng. Sci.* **1975**, *346* (1645), 139–156. https://doi.org/10.1098/rspa.1975.0170.

(71) Skarnulis, A. J.; Iijima, S.; Cowley, J. M. Refinement of the Defect Structure of `GeNb$_9$O$_{25}$' by High-Resolution Electron Microscopy. *Acta Crystallogr. A* **1976**, *32* (5), 799–805. https://doi.org/10.1107/S0567739476001630.

(72) Forghany, S. K. E.; Anderson, J. S. Reduction of the Titanium Niobium Oxides. I. TiNb$_2$O$_7$ and Ti$_2$Nb$_{10}$O$_{29}$. *J. Solid State Chem.* **1981**, *40* (2), 136–142. https://doi.org/10.1016/0022-4596(81)90373-X.

(73) Forghany, S. K. E.; Cheetham, A. K.; Olsen, A. X-Ray Microanalysis and High-Resolution Transmission Electron Microscopy of the Reduced Titanium-Niobium Oxides. *J. Solid State Chem.* **1987**, *71* (2), 305–323. https://doi.org/10.1016/0022-4596(87)90238-6.

(74) Kimura, S. Phase Equilibria in the System NbO$_2$–Nb$_2$O$_5$: Phase Relations at 1300 and 1400 °C and Related Thermodynamic Treatment. *J. Solid State Chem.* **1973**, *6* (3), 438–449. https://doi.org/10.1016/0022-4596(73)90236-3.

(75) McQueen, T.; Xu, Q.; Andersen, E. N.; Zandbergen, H. W.; Cava, R. J. Structures of the Reduced Niobium Oxides Nb$_{12}$O$_{29}$ and Nb$_{22}$O$_{54}$. *J. Solid State Chem.* **2007**, *180* (10), 2864–2870. https://doi.org/10.1016/j.jssc.2007.08.013.

(76) Rietveld, H. M. Line Profiles of Neutron Powder-Diffraction Peaks for Structure Refinement. *Acta Crystallogr.* **1967**, *22* (1), 151–152. https://doi.org/10.1107/S0365110X67000234.

(77) Rietveld, H. M. A Profile Refinement Method for Nuclear and Magnetic Structures. *J. Appl. Crystallogr.* **1969**, *2* (2), 65–71. https://doi.org/10.1107/S0021889869006558.

(78) Cheetham, A. K.; Von Dreele, R. B. Cation Distributions in Niobium Oxide Block Structures. *Nature* **1973**, *244* (139), 139–140. https://doi.org/10.1038/10.1038/physci244139a0.

(79) Von Dreele, R. B.; Cheetham, A. K. The Structures of Some Titanium-Niobium Oxides by Powder Neutron Diffraction. *Proc. R. Soc. Lond. Math. Phys. Eng. Sci.* **1974**, *338* (1614), 311–326. https://doi.org/10.1098/rspa.1974.0088.

(80) Sears, V. F. Neutron Scattering Lengths and Cross Sections. *Neutron News* **1992**, *3* (3), 26–37. https://doi.org/10.1080/10448639208218770.

(81) Gasperin, M. Affinement de la Structure de TiNb$_2$O$_7$ et Répartition des Cations. *J. Solid State Chem.* **1984**, *53* (1), 144–147. https://doi.org/10.1016/0022-4596(84)90238-X.

(82) Cheetham, A. K.; Allen, N. C. Cation Distribution in the Complex Oxide, W$_3$Nb$_{14}$O$_{44}$; a Time-of-Flight Neutron Diffraction Study. *J. Chem. Soc. Chem. Commun.* **1983**, No. 22, 1370. https://doi.org/10.1039/c39830001370.

(83) Cava, R. J.; Murphy, D. W.; Zahurak, S. M. Lithium Insertion in Wadsley–Roth Phases Based on Niobium Oxide. *J. Electrochem. Soc.* **1983**, *130* (12), 2345–2351. https://doi.org/10.1149/1.2119583.

(84) Han, J.-T.; Goodenough, J. B. 3-V Full Cell Performance of Anode Framework $TiNb_2O_7$/Spinel $LiNi_{0.5}Mn_{1.5}O_4$. *Chem. Mater.* **2011**, *23* (15), 3404–3407. https://doi.org/10.1021/cm201515g.

(85) Goodenough, J. B.; Han, J.-T. Niobium Oxide Compositions and Methods for Using Same. US 8,647,773 B2, February 11, 2014.

(86) Griffith, K. J.; Wiaderek, K. M.; Cibin, G.; Marbella, L. E.; Grey, C. P. Niobium Tungsten Oxides for High-Rate Lithium-Ion Energy Storage. *Nature* **2018**, *559* (7715), 556–563. https://doi.org/10.1038/s41586-018-0347-0.

(87) Cava, R. J.; Santoro, A.; Murphy, D. W.; Zahurak, S.; Roth, R. S. The Structures of Lithium-Inserted Metal Oxides: $LiReO_3$ and Li_2ReO_3. *J. Solid State Chem.* **1982**, *42* (3), 251–262. https://doi.org/10.1016/0022-4596(82)90004-4.

(88) Magnéli, A. Structures of the ReO_3-Type with Recurrent Dislocations of Atoms: 'Homologous Series' of Molybdenum and Tungsten Oxides. *Acta Crystallogr.* **1953**, *6* (6), 495–500. https://doi.org/10.1107/S0365110X53001381.

(89) Allpress, J. G.; Tilley, R. J. D.; Sienko, M. J. Examination of Substoichiometric WO_{3-x} Crystals by Electron Microscopy. *J. Solid State Chem.* **1971**, *3* (3), 440–451. https://doi.org/10.1016/0022-4596(71)90083-1.

(90) Koçer, C. P.; Griffith, K. J.; Grey, C. P.; Morris, A. J. Lithium Diffusion in Niobium Tungsten Oxide Shear Structures. *Chem. Mater.* **2020**, *32* (9), 3980–3989. https://doi.org/10.1021/acs.chemmater.0c00483.

(91) Zhang, L.; Zhang, X.; Tian, G.; Zhang, Q.; Knapp, M.; Ehrenberg, H.; Chen, G.; Shen, Z.; Yang, G.; Gu, L.; Du, F. Lithium Lanthanum Titanate Perovskite as an Anode for Lithium Ion Batteries. *Nat. Commun.* **2020**, *11* (1). https://doi.org/10.1038/s41467-020-17233-1.

(92) Inada, R.; Mori, T.; Kumasaka, R.; Ito, R.; Tojo, T.; Sakurai, Y. Characterization of Vacuum-Annealed $TiNb_2O_7$ as High Potential Anode Material for Lithium-Ion Battery. *Int. J. Appl. Ceram. Technol.* **2019**, *16*, 264–272. https://doi.org/10.1111/ijac.13058.

(93) Takashima, T.; Tojo, T.; Inada, R.; Sakurai, Y. Characterization of Mixed Titanium–Niobium Oxide $Ti_2Nb_{10}O_{29}$ Annealed in Vacuum as Anode Material for Lithium-Ion Battery. *J. Power Sources* **2015**, *276*, 113–119. https://doi.org/10.1016/j.jpowsour.2014.11.109.

(94) Lin, C.; Yu, S.; Zhao, H.; Wu, S.; Wang, G.; Yu, L.; Li, Y.; Zhu, Z.-Z.; Li, J.; Lin, S. Defective $Ti_2Nb_{10}O_{27.1}$: An Advanced Anode Material for Lithium-Ion Batteries. *Sci. Rep.* **2015**, *5*, 17836. https://doi.org/10.1038/srep17836.

(95) Deng, S.; Luo, Z.; Liu, Y.; Lou, X.; Lin, C.; Yang, C.; Zhao, H.; Zheng, P.; Sun, Z.; Li, J.; Wang, N.; Wu, H. $Ti_2Nb_{10}O_{29-x}$ Mesoporous Microspheres as Promising Anode Materials for High-Performance Lithium-Ion Batteries. *J. Power Sources* **2017**, *362*, 250–257. https://doi.org/10.1016/j.jpowsour.2017.07.039.

(96) Guo, B.; Yu, X.; Sun, X.-G.; Chi, M.; Qiao, Z.-A.; Liu, J.; Hu, Y.-S.; Yang, X.-Q.; Goodenough, J. B.; Dai, S. A Long-Life Lithium-Ion Battery with a Highly Porous $TiNb_2O_7$ Anode for Large-Scale Electrical Energy Storage. *Energy Environ. Sci.* **2014**, *7* (7), 2220–2226. https://doi.org/10.1039/C4EE00508B.

(97) Patoux, S.; Dolle, M.; Rousse, G.; Masquelier, C. A Reversible Lithium Intercalation Process in an ReO_3-Type Structure PNb_9O_{25}. *J. Electrochem. Soc.* **2002**, *149* (4), A391–A400. https://doi.org/10.1149/1.1455647.

(98) Yu, H.; Lan, H.; Yan, L.; Qian, S.; Cheng, X.; Zhu, H.; Long, N.; Shui, M.; Shu, J. $TiNb_2O_7$ Hollow Nanofiber Anode with Superior Electrochemical Performance in

Rechargeable Lithium Ion Batteries. *Nano Energy* **2017**, *38*, 109–117. https://doi.org/10.1016/j.nanoen.2017.05.057.

(99) Catti, M.; Pinus, I.; Knight, K. Lithium Insertion Properties of $Li_xTiNb_2O_7$ Investigated by Neutron Diffraction and First-Principles Modelling. *J. Solid State Chem.* **2015**, *229*, 19–25. https://doi.org/10.1016/j.jssc.2015.05.011.

(100) Ise, K.; Morimoto, S.; Harada, Y.; Takami, N. Large Lithium Storage in Highly Crystalline $TiNb_2O_7$ Nanoparticles Synthesized by a Hydrothermal Method as Anodes for Lithium-Ion Batteries. *Solid State Ion.* **2018**, *320*, 7–15. https://doi.org/10.1016/j.ssi.2018.02.027.

(101) Tang, K.; Mu, X.; van Aken, P. A.; Yu, Y.; Maier, J. "Nano-Pearl-String" $TiNb_2O_7$ as Anodes for Rechargeable Lithium Batteries. *Adv. Energy Mater.* **2013**, *3* (1), 49–53. https://doi.org/10.1002/aenm.201200396.

(102) Jo, C.; Kim, Y.; Hwang, J.; Shim, J.; Chun, J.; Lee, J. Block Copolymer Directed Ordered Mesostructured $TiNb_2O_7$ Multimetallic Oxide Constructed of Nanocrystals as High Power Li-Ion Battery Anodes. *Chem. Mater.* **2014**, *26* (11), 3508–3514. https://doi.org/10.1021/cm501011d.

(103) Lv, W.; Gu, J.; Niu, Y.; Wen, K.; He, W. Review—Gassing Mechanism and Suppressing Solutions in $Li_4Ti_5O_{12}$-Based Lithium-Ion Batteries. *J. Electrochem. Soc.* **2017**, *164* (9), A2213–A2224. https://doi.org/10.1149/2.0031712jes.

(104) Wang, S.; Liu, J.; Rafiz, K.; Jin, Y.; Li, Y.; Lin, Y. S. An On-Line Transient Study on Gassing Mechanism of Lithium Titanate Batteries. *J. Electrochem. Soc.* **2019**, *166* (16), A4150–A4157. https://doi.org/10.1149/2.0631916jes.

(105) Buannic, L.; Colin, J.-F.; Chapuis, M.; Chakir, M.; Patoux, S. Electrochemical Performances and Gassing Behavior of High Surface Area Titanium Niobium Oxides. *J Mater Chem A* **2016**, *4* (29), 11531–11541. https://doi.org/10.1039/C6TA03813A.

(106) Wu, X.; Lou, S.; Cheng, X.; Lin, C.; Gao, J.; Ma, Y.; Zuo, P.; Du, C.; Gao, Y.; Yin, G. Unravelling the Interface Layer Formation and Gas Evolution/Suppression on a $TiNb_2O_7$ Anode for Lithium-Ion Batteries. *ACS Appl. Mater. Interfaces* **2018**, *10* (32), 27056–27062. https://doi.org/10.1021/acsami.8b08425.

(107) Lin, C.; Yu, S.; Wu, S. Q.; Lin, S.; Zhu, Z.; Li, J.; Lu, L. $Ru_{0.01}Ti_{0.99}Nb_2O_7$ as an Intercalation-Type Anode Material with a Large Capacity and High Rate Performance for Lithium-Ion Batteries. *J Mater Chem A* **2015**. https://doi.org/10.1039/C5TA01073J.

(108) Song, H.; Kim, Y.-T. A Mo-Doped $TiNb_2O_7$ Anode for Lithium-Ion Batteries with High Rate Capability Due to Charge Redistribution. *Chem. Commun.* **2015**, *51* (48), 9849–9852. https://doi.org/10.1039/C5CC02221E.

(109) Yang, C.; Lin, C.; Lin, S.; Chen, Y.; Li, J. $Cu_{0.02}Ti_{0.94}Nb_{2.04}O_7$: An Advanced Anode Material for Lithium-Ion Batteries of Electric Vehicles. *J. Power Sources* **2016**, *328*, 336–344. https://doi.org/10.1016/j.jpowsour.2016.08.027.

(110) Park, H.; Wu, H. B.; Song, T.; David Lou, X. W.; Paik, U. Porosity-Controlled $TiNb_2O_7$ Microspheres with Partial Nitridation as A Practical Negative Electrode for High-Power Lithium-Ion Batteries. *Adv. Energy Mater.* **2015**, *5* (8), 1401945. https://doi.org/10.1002/aenm.201401945.

(111) Takami, N.; Inagaki, H.; Kishi, T.; Harada, Y.; Fujita, Y.; Hoshina, K. Electrochemical Kinetics and Safety of 2-Volt Class Li-Ion Battery System Using Lithium Titanium Oxide Anode. *J. Electrochem. Soc.* **2009**, *156* (2), A128. https://doi.org/10.1149/1.3043441.

(112) Harada, Y.; Hoshina, K.; Inagaki, H.; Takami, N. Influence of Synthesis Conditions on Crystal Formation and Electrochemical Properties of $TiO_2(B)$ Particles as Anode Materials for Lithium-Ion Batteries. *Electrochimica Acta* **2013**, *112*, 310–317. https://doi.org/10.1016/j.electacta.2013.08.148.

(113) Takami, N.; Ise, K.; Harada, Y.; Iwasaki, T.; Kishi, T.; Hoshina, K. High-Energy, Fast-Charging, Long-Life Lithium-Ion Batteries Using $TiNb_2O_7$ Anodes for Automotive Applications. *J. Power Sources* **2018**, *396*, 429–436. https://doi.org/10.1016/j.jpowsour.2018.06.059.

(114) Harada, Y.; Sasakawa, T.; Takami, N.; Ishida, N.; Kitamura, N.; Idemoto, Y. Structural Modification on Lithium Host Site in $Li_2(Sr_{1-x}Na_x)Ti_{6-x}Nb_xO_{14}$ ($0 \leq x \leq 1$) Anode Material for Lithium-Ion Batteries. In *AiMES 2018 Meeting*; The Electrochemical Society: Cancun, Mexico, 2018; Vol. 1, p 421. http://toc.proceedings.com/41414webtoc.pdf (accessed May 07, 2020).

(115) Harada, Y.; Takami, N.; Inagaki, H.; Yoshida, Y. Battery Active Material, Nonaqueous Electrolyte Battery and Battery Pack. US 9,515,319 B2, December 6, 2016.

(116) Zhu, C.; Usiskin, R. E.; Yu, Y.; Maier, J. The Nanoscale Circuitry of Battery Electrodes. *Science* **2017**, *358* (6369), eaao2808. https://doi.org/10.1126/science.aao2808.

(117) Cheng, Q.; Liang, J.; Lin, N.; Guo, C.; Zhu, Y.; Qian, Y. Porous $TiNb_2O_7$ Nanospheres as Ultra Long-Life and High-Power Anodes for Lithium-Ion Batteries. *Electrochimica Acta* **2015**, *176*, 456–462. https://doi.org/10.1016/j.electacta.2015.07.038.

(118) Finegan, D. P.; Tjaden, B.; M. M. Heenan, T.; Jervis, R.; Michiel, M. D.; Rack, A.; Hinds, G.; Brett, D. J. L.; Shearing, P. R. Tracking Internal Temperature and Structural Dynamics during Nail Penetration of Lithium-Ion Cells. *J. Electrochem. Soc.* **2017**, *164* (13), A3285–A3291. https://doi.org/10.1149/2.1501713jes.

(119) CBMM fecha parceria com Toshiba para producao de baterias automotivas https://br.reuters.com/article/mineracao-cbmn-baterias-idBRKBN1JL2Q5-OBRBS (accessed Sep 3, 2020).

(120) Eric Onstad. BMW to buy cobalt direct from Australia, Morocco for EV batteries https://www.reuters.com/article/us-bmw-electric-cobalt/bmw-to-buy-cobalt-direct-from-australia-morocco-for-ev-batteries-idUSKCN1RZ1RK (accessed Sep 3, 2020).

(121) Yilei Sun; Melanie Burton. "Please mine more nickel," Musk urges as Tesla boosts production https://www.reuters.com/article/us-tesla-nickel/please-mine-more-nickel-musk-urges-as-tesla-boosts-production-idUSKCN24O0RV (accessed Sep 3, 2020).

(122) Michael Herh. LG Chem Joins a Global Project to Trace Cobalt Through a Blockchain Platform http://www.businesskorea.co.kr/news/articleView.html?idxno=28428 (accessed Sep 3, 2020).

(123) Griffith, K. J.; Grey, C. P. Superionic Lithium Intercalation through 2×2 nm^2 Columns in the Crystallographic Shear Phase $Nb_{18}W_8O_{69}$. *Chem. Mater.* **2020**, *32* (9), 3860–3868. https://doi.org/10.1021/acs.chemmater.9b05403.

(124) Koçer, C. P.; Griffith, K. J.; Grey, C. P.; Morris, A. J. Cation Disorder and Lithium Insertion Mechanism of Wadsley–Roth Crystallographic Shear Phases from First Principles. *J. Am. Chem. Soc.* **2019**, *141* (38), 15121–15134. https://doi.org/10.1021/jacs.9b06316.

Author Biographies

Kent J. Griffith earned his B.S. in Chemistry from Indiana University in 2013 and then moved to Cambridge, England on a Churchill Scholarship. He obtained a Ph.D. in Chemistry under the supervision of Clare Grey at the University of Cambridge in 2018 before moving back to the U.S. to undertake post-doctoral research at Northwestern University. His research interests include structure–property relationships in functional inorganic materials for energy storage and conversion applications.

Yasuhiro Harada obtained his Ph.D. in Inorganic Chemistry from Tokyo University of Science in 2002 under the supervision of Prof. Jun Kuwano who studied under Prof. A. R. West of the University of Sheffield. After completing his Ph.D., he joined Toshiba Research and Development Center and his interests focus on the development of new anode materials for lithium ion batteries. He is currently a senior fellow of Nano Materials and Frontier Research Laboratories.

Shun Egusa earned his Ph.D. in Polymer Chemistry from Kyoto University. He joined Toshiba Corporation in 1985 as a material researcher in the R&D center. He transferred to Toshiba Cambridge Research Ltd. as deputy managing director in 1997. He has been involved in the battery business since 2007 and became a head of the battery factory in Japan. From 2019, he has been Vice President of the Battery Business Division at the Toshiba Head Office.

Rogério Ribas earned his B.S. in Chemical Engineering and his Master's Degree in Chemical Engineering from the Federal University of Uberlândia. He then earned an MBA in Business Administration and Management from University of Pittsburgh, Joseph M. Katz Graduate School of Business. He is currently the Executive Manager for Battery Products at CBMM with over 20 years of experience in applied technologies.

Robson S. Monteiro earned his Ph.D. degree in Chemical Engineering from the Federal University of Rio de Janeiro and was a post-doctoral Fellow at Worcester Polytechnic Institute. He then worked as a Research Scientist for Hyperion Catalysis International (Cambridge, MA) in the industrial production of carbon nanotubes. He is currently Senior Market Development Specialist for CBMM with more than 20 years of experience on RD&I projects related to catalytic, energy storage, and energy conversion materials.

Robert Von Dreele obtained a B.S. in Chemical Engineering in 1966 and a Ph.D. in Chemistry from Cornell University in 1971. He then started as Assistant Professor of Chemistry at Arizona State University. During that time, he also did a National Science Foundation post-doctoral year (1972–1973) at Oxford University with Prof. J. S. Anderson during which he began his life's work on the analysis of powder diffraction data.

Tony Cheetham earned his B.A. and D.Phil. degrees at Oxford and then held a post-doctoral fellowship at Lincoln College, Oxford, and the Materials Physics Division, A.E.R.E. Harwell. He has held faculty positions at Oxford, UC Santa Barbara, Cambridge, and the National University of Singapore. Cheetham's research interests include: structural characterization of materials using

advanced diffraction and NMR methods, zeolitic aluminosilicates and phosphates, defects in transition metal oxides, physical properties of metal-organic frameworks, and hybrid perovskites.

Robert Cava received his Ph.D. from MIT in 1978, after which he was an NRC post-doctoral scientist at NIST. He is currently the Russell Wellman Moore Professor of Chemistry at Princeton University, and was previously Chair of the Chemistry Department and Director of the Materials Institute. He was a Distinguished Member of Technical Staff at Bell Labs and is a member of the US National Academy of Sciences and Foreign Member of The Royal Society.

Clare P. Grey received a B.A. and D.Phil. from Oxford University and was a post-doctoral fellow at Nijmegen and at DuPont CR&D. She joined the faculty at Stony Brook University in 1994, moving to Cambridge University in 2009 where she is the Geoffrey-Moorhouse-Gibson and Royal Society Professor of Chemistry. Her research interests include the use of solid-state NMR and diffraction to determine structure–function relationships in materials for energy storage, conversion and for carbon capture.

John Bannister Goodenough received a B.A. in Mathematics from Yale University in 1943 and a Ph.D. in Physics from the University of Chicago in 1952. He was a Research Scientist and Group Leader at the MIT Lincoln Laboratory until 1976 and Professor and Head of the Inorganic Chemistry Laboratory in Oxford, England until 1986. He is currently the Virginia H. Cockrell Centennial Professor of Materials Science and Engineering at the University of Texas at Austin.

For Table of Contents only